AD-A111 801 NAVAL TRAINING EQUIPMENT CENTER ORLANDO FL F/G 5/9
VISUAL TECHNOLOGY RESEARCH SIMULATOR, VISUAL AND MOTION SYSTEM --ETC(U)
APR 81 G B BROWDER, S K BUTRIMAS
UNCLASSIFIED NAVTRAEQUIPC-IH-326 NL

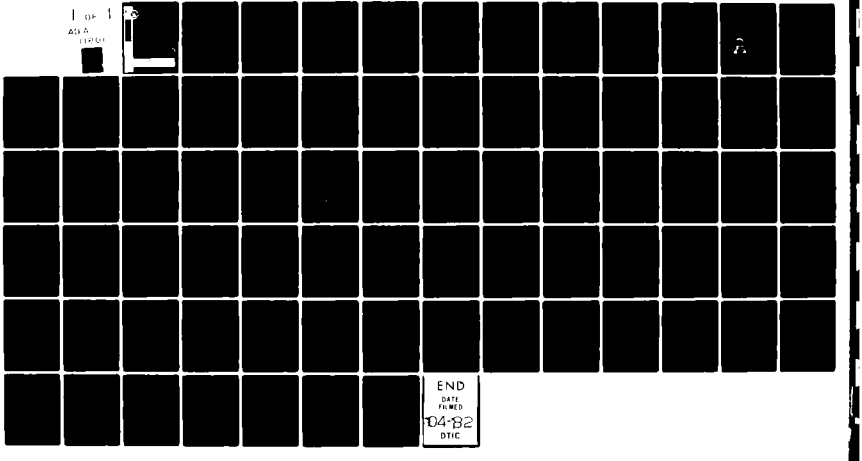

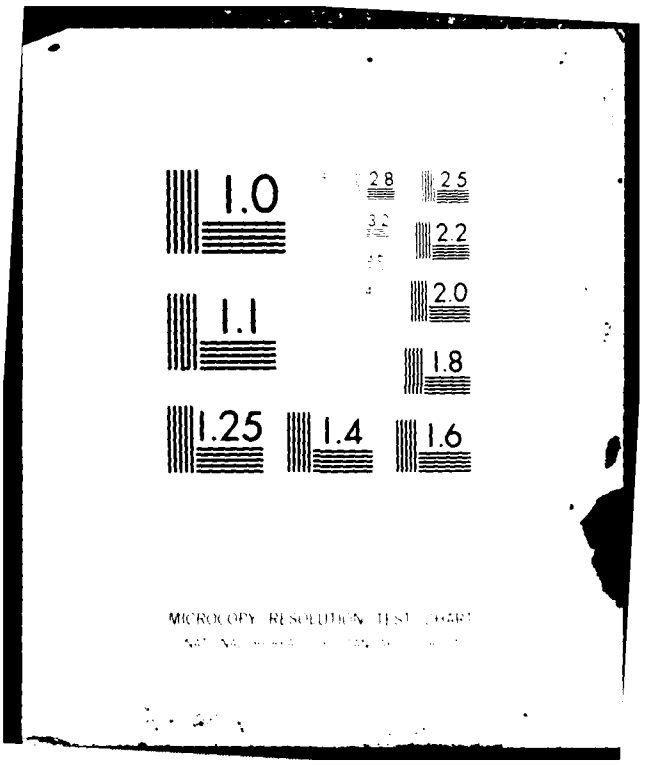
1.0
2.8
2.5
3.2
2.2
1.1
2.0
1.8
1.25
1.4
1.6
MICROCOPY RESOLUTION TEST

(12)
4-3

TECHNICAL REPORT: NAVTRAEQUIPCEN IH-326

# VISUAL TECHNOLOGY RESEARCH SIMULATOR VISUAL AND MOTION SYSTEM DYNAMICS

G. Blair Browder
Steve K. Butrimas
Naval Training Equipment Center

April 1981



NAVAL TRAINING EQUIPMENT CENTER
ORLANDO, FLORIDA 32813

UNCLASSIFIED

SECURITY CLASSIFICATION OF THIS PAGE (When Data Entered)

| REPORT DOCUMENTATION PAGE | READ INSTRUCTIONS BEFORE COMPLETING FORM |
|---|---|
| 1. REPORT NUMBER: NAVTRAEQUIPCEN IH-326 | 2. GOVT ACCESSION NO.: AD-A111801 |
| 3. RECIPIENT'S CATALOG NUMBER: | |
| 4. TITLE (and Subtitle): VISUAL TECHNOLOGY RESEARCH SIMULATOR VISUAL AND MOTION SYSTEM DYNAMICS | 5. TYPE OF REPORT & PERIOD COVERED: INTERIM 1978-1981 |
| | 6. PERFORMING ORG. REPORT NUMBER: |
| 7. AUTHOR(s): G. Blair Browder, Steve K. Butrimas | 8. CONTRACT OR GRANT NUMBER(s): |
| 9. PERFORMING ORGANIZATION NAME AND ADDRESS: Visual Technology Research Simulator, Naval Training Equipment Center, Orlando, FL 32813 | 10. PROGRAM ELEMENT, PROJECT, TASK AREA & WORK UNIT NUMBERS: NAVTRAEQUIPCEN Task No. 0785 |
| 11. CONTROLLING OFFICE NAME AND ADDRESS: Commanding Officer, Naval Training Equipment Center, Orlando, FL 32813 | 12. REPORT DATE: April 1981 |
| | 13. NUMBER OF PAGES: 71 |
| 14. MONITORING AGENCY NAME & ADDRESS (if different from Controlling Office) | 15. SECURITY CLASS. (of this report): UNCLASSIFIED |
| | 15a. DECLASSIFICATION/DOWNGRADING SCHEDULE |

16. DISTRIBUTION STATEMENT (of this Report)

Approved for public release, distribution unlimited.

17. DISTRIBUTION STATEMENT (of the abstract entered in Block 20, if different from Report)

18. SUPPLEMENTARY NOTES

19. KEY WORDS (Continue on reverse side if necessary and identify by block number)

Computer Image Generation
Model Board Image Generation
Servo Response
Linkage
Motion Simulation
Visual Simulation
Time Lag
Visual Technology Research Simulator

20. ABSTRACT (Continue on reverse side if necessary and identify by block number)

Simulator system time lags and transport delays can be critical factors in achieving a successful modern trainer. This document presents the results of detailed measurements made on the Navy's Visual Technology Research Simulator (VTRS/CTOL). These measurements determined "end-to-end" dynamic lags, with aircraft control stick as the input stimulus and visual/motion hardware response as the output. Major subsystems of the VTRS/CTOL include a T-2C aircraft cockpit, pneumatic G-seat, six degree of freedom motion base, wide-

DD FORM 1 JAN 73 1473 EDITION OF 1 NOV 65 IS OBSOLETE
S/N 0102-014-6601

UNCLASSIFIED

SECURITY CLASSIFICATION OF THIS PAGE (When Data Entered)

angle dome display with a servo-controlled projection system driven with either CIG or closed circuit model board TV. Dynamic performance data shows phasing between the motion and visual systems for CIG and model board simulation. This study concludes that the VTRS/CTOL simulator throughput lags are less than 150 milliseconds which is generally accepted as satisfactory for simulation.

# PREFACE

This document was published to provide a comprehensive reference for the dynamic response of the visual and motion systems of the CTOL simulator at the Visual Technology Research Simulator (VTRS). Transmission delays from control stick stimulus to hardware system and video output are evaluated. These measurements were made not only to quantitatively evaluate the dynamic matching of all subsystems, but to provide the experimentor with a reference for his analyses.

This document defines "end-to-end" dynamics of the current VTRS/CTOL visual/motion systems, and extrapolates performance to CIG systems with comprehensive distortion correction which is being implemented.

The authors are indebted to Max Coombes and Jack Edgar for their technical assistance during this task, and to Walter Chambers for his consultation.

TABLE OF CONTENTS


| Section | | Page |
|---|---|---|
| | INTRODUCTION | 7 |
| I | LINKAGE AND COMPUTER SYSTEM | 9 |
| | SYSTEM DESCRIPTION | 9 |
| | THROUGHPUT: CONTROL STICK TO MOTION/G-SEAT | 13 |
| | THROUGHPUT: CONTROL STICK TO TIP SERVOS | 14 |
| | THROUGHPUT: CONTROL STICK TO PROBE SERVOS | 14 |
| | THROUGHPUT: (1) CONTROL STICK TO CIG INPUT AND (2) CIG INPUT TO VIDEO OUTPUT | 14 |
| II | VISUAL SERVO SYSTEMS | 16 |
| | VIDEO SYSTEMS | 16 |
| | VISUAL SERVO SYSTEMS DESCRIPTION | 16 |
| | SERVOS COMMON TO TIG OPERATIONS | 16 |
| | FRESNEL LENS OPTICAL LANDING SYSTEM | 16 |
| | SERVOS COMMON TO CIG AND TIG OPERATIONS | 16 |
| | SUMMARY OF SERVO SYSTEMS EVALUATED | 16 |
| | SERVO PERFORMANCE CRITERIA | 17 |
| | FREQUENCY RESPONSE | 17 |
| | STEP RESPONSE | 20 |
| | VISUAL SERVO PERFORMANCE | 20 |
| | TIP SERVOS | 20 |
| | Frequency Response | 20 |
| | Step Response | 22 |
| | Static Repeatability | 22 |
| | FLOLS SERVOS | 22 |
| | Frequency Response | 22 |
| | Step Response | 24 |
| | Static Repeatability | 25 |
| | GANTRY RATE SERVOS | 25 |
| | Frequency Response | 25 |
| | Step Response | 27 |
| | Static Repeatability | 27 |
| | PROBE SERVO | 27 |
| | Frequency Response | 27 |
| | Step Response | 29 |
| | Static Repeatability | 30 |
| III | THE MOTION SYSTEM | 31 |
| | MOTION PLATFORM DESCRIPTION AND OPERATING LIMITATIONS | 31 |
| | MOTION SYSTEM SOFTWARE | 32 |
| | SYSTEM SOFTWARE | 32 |
| | Aircraft Drives | 33 |
| | Pitch | 33 |
| | Roll | 37 |
| | Yaw | 38 |
| | Longitudinal Translation | 39 |
| | Lateral Motion Drive | 41 |
| | Vertical Motion Drive | 42 |
| | GENERATION OF ACCELERATION CUES | 44 |
| | MOTION PLATFORM PERFORMANCE | 44 |

TABLE OF CONTENTS (Con't.)


| Section | | Page |
|---|---|---|
| IV | THE "G"-SEAT SYSTEM. . . . . | 47 |
| V | SYSTEM RESPONSE SUMMARY. . . . . | 50 |
| VI | DESIGN FEATURES SUMMARY. . . . . | 53 |
| | REFERENCES . . . . . | 55 |
| **Appendix** | | |
| A | TECHNICAL DATA AND ALGORITHMS FOR ACCELERATION CUE GENERATION OF THE MOTION SYSTEM . . . . . | 57 |

# LIST OF ILLUSTRATIONS


| Figure | | Page |
|---|---|---|
| I-1 | VTRS System Diagram | 10 |
| I-2 | CPU Phasing Diagram | 11 |
| I-3 | Flight and Visual Linkage Process | 12 |
| I-4 | System Throughput Test Diagram. | 13 |
| II-1 | Servo in Test Configuration | 18 |
| II-2 | Continuous Type Servos With Sin-Cos Potentiometer | 18 |
| II-3 | TIP Servos - Frequency Responses (Magnitude). | 20 |
| II-4 | TIP Servos - Frequency Responses (Phase). | 21 |
| II-5 | Target Projector Servo Responses to Step Inputs | 22 |
| II-6 | FLOLS Servos - Frequency Responses (Magnitude). | 23 |
| II-7 | FLOLS Servos - Frequency Responses (Phase). | 23 |
| II-8 | FLOLS Servo Responses to Step Inputs. | 24 |
| II-9 | GANTRY Rate Servos - Frequency Responses (Magnitude). | 25 |
| II-10 | GANTRY Rate Servos - Frequency Responses (Phase). | 26 |
| II-11 | GANTRY Servo Responses to Step Rate Inputs. | 27 |
| II-12 | PROBE Servos - Frequency Responses (Magnitude). | 28 |
| II-13 | PROBE Servos - Frequency Responses (Phase). | 28 |
| II-14 | PROBE Servo Responses to Step Inputs. | 29 |
| III-1 | VTRS Motion Platform Depicting Hydraulic Actuators and Fluid Distribution System. | 31 |
| III-2 | Motion Parameter Flow | 33 |
| III-3 | Platform Pitch Software | 35 |
| III-4 | Pitch Gravity Align Due to Aircraft Longitudinal Acceleration Step Input. | 35 |
| III-5 | Pitch Gravity Align Due to Aircraft Longitudinal Acceleration Step Input. | 36 |
| III-6 | Pitch Onset Due to Aircraft Angle of Attack Step Input. | 36 |
| III-7 | Platform Roll Software. | 37 |
| III-8 | Roll Onset Due to Aircraft Roll Rate Step Input | 38 |
| III-9 | Platform Yaw Software | 38 |
| III-10 | Yaw Onset Due to Aircraft Sideslip Angle Step Input | 39 |
| III-11 | Platform Longitudinal Software. | 40 |
| III-12 | Longitudinal Onset Due to Aircraft X-Axis Step Inputs | 40 |
| III-13 | Platform Lateral Software | 41 |
| III-14 | Lateral Onset Due to Aircraft Yaw Rate. | 42 |
| III-15 | Platform Vertical Software. | 43 |
| III-16 | Vertical Onset Due to Aircraft Z-Axis Step Input. | 43 |
| III-17 | Effect of Increased Filter Bandwidth of Onset Cuing Characteristics. | 44 |
| III-18 | Effect of Increased Filter Bandwidth of Onset Cuing Characteristics. | 44 |
| IV-1 | Cell Calibration Curve. | 47 |
| IV-2 | Frequency Response of G-Seat Cell with Load | 48 |
| IV-3 | Cell Position Response to Step Command. | 48 |
| V-1 | VTRS Dynamic Response | 50 |
| V-2 | VTRS Dynamic Response for CIG Systems | 51 |
| A-1 | Effect of Increasing Motion Leg Filter Bandwidth. | 57 |

LIST OF ILLUSTRATIONS (Con't.)


| Figure | | Page |
|---|---|---|
| A-2 | Platform Longitudinal Block Diagram | 58 |
| A-3 | Platform Lateral Block Diagram | 59 |
| A-4 | Platform Vertical Block Diagram | 59 |
| A-5 | Platform Roll Block Diagram | 60 |
| A-6 | Platform Pitch Block Diagram | 60 |
| A-7 | Platform Yaw Block Diagram | 61 |
| A-8 | First Order Filter Response | 63 |
| A-9 | Position Response for Step Input | 64 |
| A-10 | Typical Filter Velocity and Acceleration Outputs | 64 |
| A-11 | Onset Cue Velocity and Acceleration Response | 65 |
| A-12 | Motion System Test Diagram | 65 |
| A-13 | Motion System Frequency Response | 66 |
| A-14 | Frequency Response of Motion Base Acceleration Onset Cue | 67 |
| A-15 | Motion System Heave Step Response | 68 |
| A-16 | Gravity Align | 69 |
| A-17 | Generalized Gravity Align Frequency Response | 69 |
| A-18 | Generalized Frequency Response for Acceleration Onset | 70 |
| A-19 | Onset Acceleration Performance | 71 |


LIST OF TABLES


| Table | | Page |
|---|---|---|
| I-1 | LINKAGE THROUGHPUT MEASUREMENTS | 13 |
| II-1 | VISUAL SERVOS PERFORMANCE SUMMARY - TIP | 21 |
| II-2 | VISUAL SERVOS PERFORMANCE SUMMARY - FLOLS | 24 |
| II-3 | VISUAL SERVOS PERFORMANCE SUMMARY - GANTRY | 26 |
| II-4 | VISUAL SERVOS PERFORMANCE SUMMARY - PROBE | 29 |
| III-1 | PLATFORM OPERATING LIMITATIONS | 32 |

# INTRODUCTION

This report presents dynamic performance measurements made at the Navy's Visual Technology Research Simulator (VTRS) facility, and shows timing interactions between visual and motion subsystems of the Conventional Take-Off and Landing (CTOL) simulator.

Major subsystems of the VTRS/CTOL include a T2C aircraft cockpit with G-seat mounted on a six degree of freedom motion base and a wide angle dome display. The display consists of a wide angle background TV projector and a servo controlled target TV projector. The simulator's displays receive video from either computer image generation (CIG) or closed circuit model board TV system and other TV special effects equipment.

The simulator's computer system is composed of 3 Systems Engineering Laboratories (SEL) 32/75 Central Processing Units (CPU). Flight and Visual CPU's are controlled by an Executive CPU which also communicates with the Experimenter/Operator control station. The flight and visual computations considered in this report are all performed at a 30 Hz rate. The relationship of these CPUs is discussed later in detail.

This report is divided into six sections, presenting detailed dynamic performance measurements of the following VTRS systems:

a. Linkage and computer system delays from control stick input to all major output hardware. The output hardware includes the projection servos, the TV camera/probe gantry servos, the motion platform and G-seat, and the CIG.

b. Visual servo performance for target projector servos used in display and for servos used in image generation by the closed circuit model board TV system.

c. Motion platform performance including analyses of the servo controlled legs and of the software algorithms that generate the onset acceleration and sustained acceleration (G-align) cuing.

d. G-seat transient and frequency response under typical loaded conditions used to generate sustained acceleration cues.

e. System Response Summary.

f. Design Features Summary.

# SECTION I

# LINKAGE AND COMPUTER SYSTEM

## SYSTEM DESCRIPTION

The VTRS/CTOL simulator incorporates a linkage system which connects the simulator input cockpit controls (i.e., throttle, control stick, rudder and toe brakes) to the computers and back out to all simulator output hardware. The linkage system includes the functions of signal sampling, analog to digital conversion, storage, data transfer, data distribution, digital to analog conversion and signal smoothing. Linkage transport delays (throughput delays) were measured between the analog input stimulus (control movement) and the output to subsystem hardware. The linkage is shown in the system diagram (Figure I-1).

Linkage throughput delays were measured over the following transmission routes, some of which apply to Computer Image Generation (CIG), some to the model board Target Image Generation (TIG) and some of which are common to both CIG and TIG operations:

a. Cockpit control to motion base (leg servos)

b. Cockpit control to G-seat bellows servos

c. Cockpit control to Target Imagery Projector (TIP) servos

d. Cockpit control to TIG (probe and gantry servos)

e. Cockpit control to CIG input and to CIG video output

The first three linkage routes, the motion base, G-seat and TIP servos are common to both CIG and TIG.

The function of the linkage system is to provide two-way communication between computer memory and simulator hardware.

Major components of the linkage are:

a. The master controller which is the control center

b. System cards which service the hardware systems, and

c. The subcontroller which serves as the interface between the master controller and the system cards.

The master controller transfers output data in serial form from an internal buffer memory to the designated system card, and simultaneously accepts input data from the system card and stores it in the buffer memory.

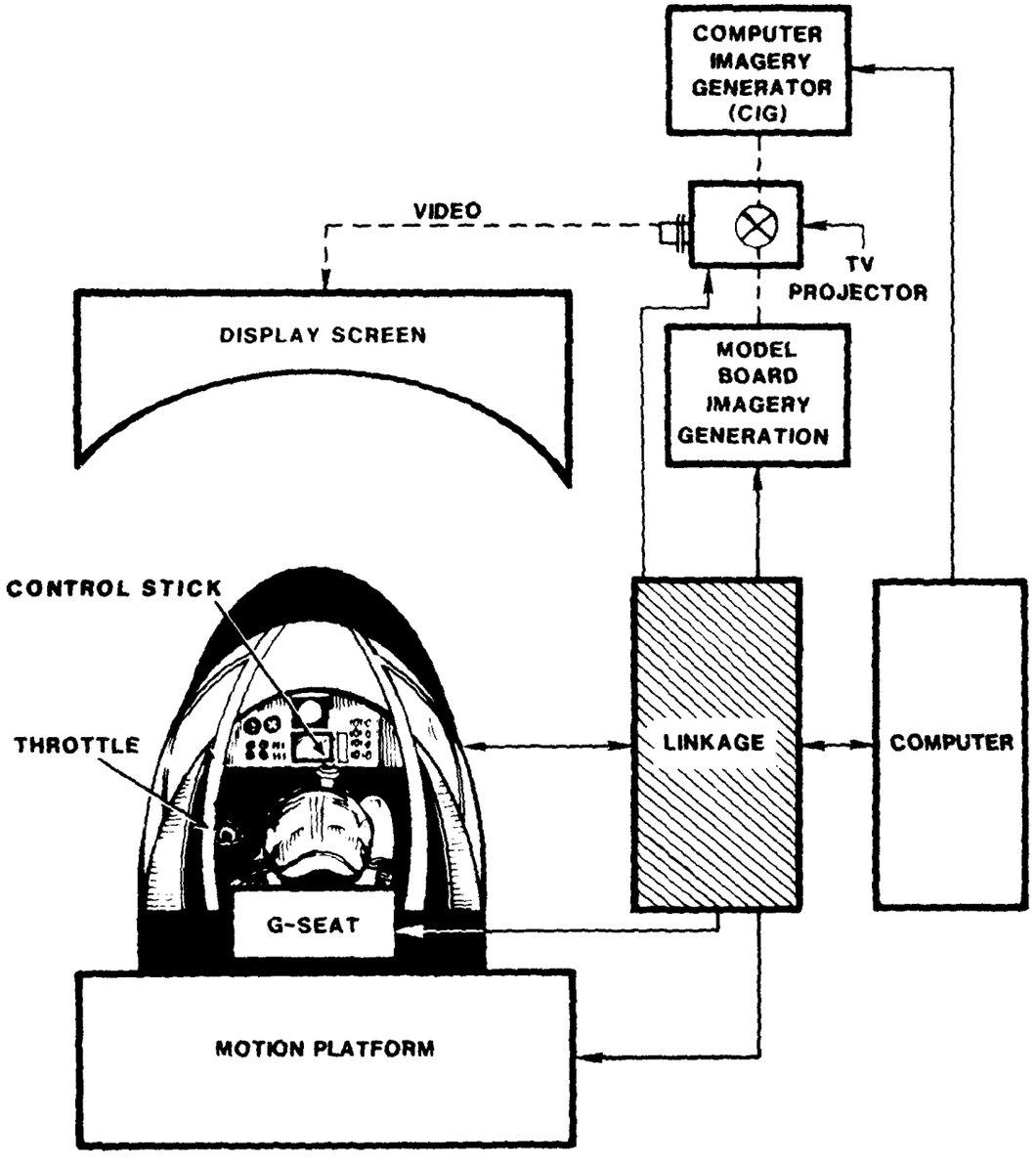


Figure I-1. VTRS System Diagram

System cards provide analog and digital conversion and interconnection functions required by the system being serviced.

The simulator's computer system consists of three SEL 32/75 computers: one CPU for Executive/Experimentor-Operator operations (EO), one CPU for computation of flight dynamics/kinematics, and the third CPU for visual computations. Computation rate, relative phasing between the computation frames of the visual and flight CPU's, and their associated linkage transfers are major contributors to throughput delay.

Figure I-2 shows the timing relationships between the flight and visual CPU's and their associated linkage transfers of data from hardware to computer memory and from computer memory to hardware. All computational measurements were made with the software operating at 30 frames per second update rate (a computation period of 33.33 milliseconds). Computation frames are divided into 4 subframes, each of 8.33 milliseconds duration. The visual CPU frame lags the flight CPU frame by two subframes. This flight/visual CPU phasing minimizes lag in the visual computation, since the most recent flight outputs are computed by end of flight's second subframe and are immediately used by the visual CPU.

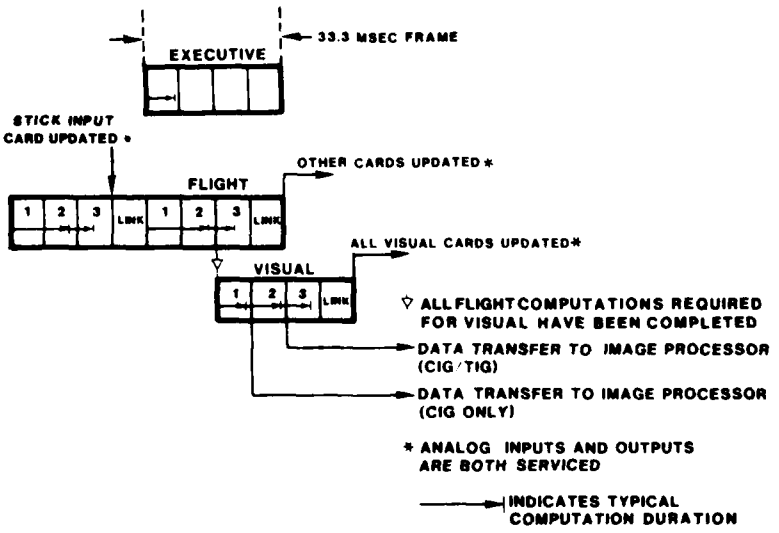


Figure I-2. CPU Phasing Diagram

There are two linkage data transfer subframes, a flight linkage transfer and a visual linkage transfer (See Figure I-3). Flight linkage performs a special service of System Card No. 135 which contains the aircraft control stick inputs plus rudder and toe brakes. The control stick input is serviced up front in the cycle to minimize delay between stick input and transfer to

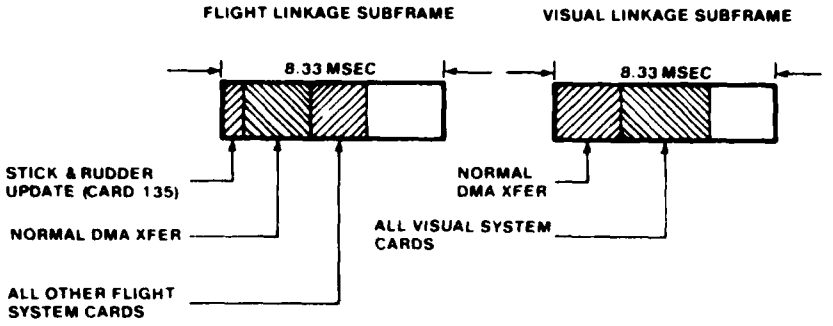


Figure I-3. Flight and Visual Linkage Process

computer memory. The flight linkage process is initiated with the update of System Card No. 135, followed immediately with the Direct Memory Access (DMA) transfer with common CPU memory and finally an update of all other flight System Cards. These other flight cards are predominantly output cards serviced during subframe 4 to output commands computed during subframes 1, 2, and 3 and transferred from common CPU memory during the DMA. The visual linkage sequence is a DMA transfer out of common CPU memory followed by update of all visual System Cards. During simultaneous CIG/TIG operation, data is transferred to the CIG at the end of visual CPU subframe 2. In general, each linkage process is completed in less than 4 milliseconds.

Data transfers to the CIG are a serial data transfer from the SEL 32/75 visual buffer memory to the CIG's computer memory. For CIG only operation data transfer occurs at the end of subframe 1 of the visual frame (Figure I-2). Three-dimensional computations are performed in the Programmable Data Processor (PDP) 11/55 and then data is transferred to General Electric's special purpose image processor (CIG frame II and III hardware) for conversion to a two-dimensional video picture.

The basic test set-up used for throughput determination is shown in Figure I-4. A control stick analog input was generated as a square wave using the Servomatic Analyzer. The frequency of the square wave input was set at approximately 3.82 Hz, producing step changes every 131 milliseconds. Since the time between step changes was not an integer number of computational frames, step inputs occurred at slightly different times with respect to the flight and visual frames. Four computer frames are 133 milliseconds duration; therefore, the input step changes occurred at about 2 milliseconds out of phase with a four-frame cycle and tended to "walk" with respect to each frame.

This "walking" of the control stick step input assured the occurrence of minimum and maximum throughput cases. The minimum throughput occurred when the control stick input changed state immediately before it was sampled by the A/D (System Card No. 135). The maximum throughput occurred when the control stick input changed state immediately after the A/D service. Since in this case the A/D servicing of the input was just missed, a full frame (cycle) must go by before the next A/D sample. Thus, the difference between minimum and

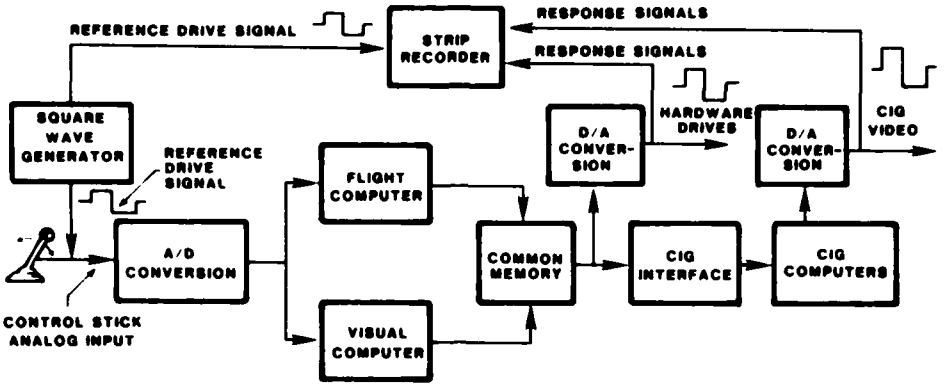


Figure I-4. System Throughput Test Diagram

maximum throughput was 33.3 milliseconds. A summary of throughput measurements from control stick to each major hardware subsystem is presented in Table I-1 below.

Aerodynamic and other computational lags (filters) were removed from the flight and visual software so that all transport delay measurements reflect only computer and linkage induced lags.

Flight and visual dynamics are computed at 30 Hz, more than 10 times the maximum system bandwidth. Thus computational sampling lags are small in comparison to the measured throughput delays.

TABLE I-1
LINKAGE THROUGHPUT MEASUREMENTS

| | |
|---|---|
| Control Stick to Motion BASE and G-seat | 55 ± 17 msec |
| Control Stick to TIP Servos | 68 ± 17 msec |
| Control Stick to Probe and Gantry Servos | 68 ± 17 msec |
| Control Stick to SEL/PDP-11 Data Transfer (CIG only mode) | 50 ± 17 msec |
| Control Stick to SEL/PDP-11 Data Transfer (CIG/TIG mode) | 58 ± 17 msec |

THROUGHPUT: CONTROL STICK TO MOTION/G-SEAT

Throughput measurements were made from the cockpit control stick input to the motion base and G-seat analog drive signals. The motion base drive signal for this throughput measurement was the input signal to the leg servo pre-filters. The visual CPU does not contribute to the throughput delay, since all computation takes place in the flight CPU. Motion base drive signals are transmitted during the flight DMA transfer. The G-seat throughput

route is the same as that of the motion system. Throughput measurements from control stick input to the motion base drive signals indicate a transport delay of 55 ± 17 msec.

THROUGHPUT: CONTROL STICK TO TIP SERVOS

Throughput measurements were made from the cockpit control stick input to the TIP servo drive signals. These analog drive signals are computed in both the flight and visual CPUs. TIP servo drive signals are transmitted during the visual DMA transfer. Throughput measurements from the control stick input to the TIP servo drives indicated a transport delay of 68 ± 17 msec.

THROUGHPUT: CONTROL STICK TO PROBE SERVOS

Throughput measurements were made from the control stick input to the probe servos drive signals. These analog signals were measured at the input to the probe pre-filter networks (designed to smooth desampling noise). Computations are performed in both the flight and visual CPUs with probe drive signals transmitted during the visual DMA transfer. Throughput measurements from control stick input to the probe servos drive signals indicated a transport delay of 68 ± 17 msec.

THROUGHPUT: (1) CONTROL STICK TO CIG INPUT AND (2) CIG INPUT TO VIDEO OUTPUT

Throughput from control stick input to video output can be logically divided into two throughput segments, (1) control stick input to CIG data input, and (2) CIG data input to video output. Video output was acknowledged as the presence of video signal in the first horizontal line of the raster which is the first pixel of CIG video. An additional video time period equal to one raster field (17 msec) will be considered later as a rise time equivalent when transport delays and hardware time constants are combined to produce total "system lags". The two throughputs were determined by first measuring the total throughput from control stick to video output and then by measuring the segment from CIG input to video output. The remaining throughput segment from control stick input to CIG data input was then computed by subtracting the partial throughput from the total (end-to-end).

The flight and visual computations were modified such that the entire scene viewed from the eyepoint would switch alternately from black to white depending on polarity of the control stick input. A flag in the visual computer was programmed to change status upon reception of a change of control stick polarity. The scene correspondingly was programmed to instantly change from black to white upon change in status of the visual flag. Therefore, the throughput measurement did not include intentional aerodynamic and kinematic lags in flight and visual computations. The throughput measurement from control stick input to CIG video output was found to be 108 ± 17 msec. A throughput measurement was also made from the CIG input (to the PDP-11) to the CIG video output using the same computational scheme just described for the total throughput path from control stick input to CIG video output. This partial throughput measurement indicated 50 msec. In other words, three CIG computational frames (60 Hz) are used to convert the eyepoint data into a three dimensional view and then finally into a two dimensional video signal.

In summary, the CIG throughput measurements from control stick input to the CIG input (to the PDP-11) were:

CIG Mode Only = 50 ± 17 msec
CIG/TIG Mode = 58 ± 17 msec

Throughput from the CIG input to the first pixel of CIG video output was determined to be 50 msec. An additional time period of one TV field of 17 msec is considered a rise time equivalent.

Table I-1 summarizes all of the linkage and computer system throughput measurements discussed in this section.

# SECTION II

# VISUAL SERVO SYSTEMS

## VIDEO SYSTEMS

In the CIG mode, the target image is generated through computer update of a data base. In the TIG mode, the target image is generated by viewing a model board through a closed circuit TV system. Images created by either mode are displayed on the screen by a high intensity TV projector and appropriate optics. The target image is positioned on the screen by servo control of the projector optical elements.

A Fresnel Lens Optical Landing System (FLOLS) is simulated in both CIG and TIG modes and provides imagery signals independent of the other two video systems. In other words, TIG carrier depiction could have either CIG or TIG FLOLS, or vice versa. In some cases, both FLOLS modes can be used simultaneously.

Target image motion is accomplished by servo systems interfacing software generated signals from CIG and TIG modes to hardware systems which respond to pilot generated commands from the cockpit controls.

## VISUAL SERVO SYSTEMS DESCRIPTION

SERVOS COMMON TO TIG OPERATIONS. The probe, which houses the TV camera and associated optical systems, is driven over the model board by a three-axis gantry servo. As the probe is positioned to simulate aircraft position, line-of-sight between the model and focal plane of the camera is maintained by a servo controlled prism system. Heading and pitch servos keep the model within the field of view of the camera while a roll servo maintains desired roll attitude of the received image.

FRESNEL LENS OPTICAL LANDING SYSTEM. The Fresnel Lens Optical Landing System (FLOLS) is simulated by optically combining a FLOLS model image with the target projector image for dome presentation. A position servo on the FLOLS model controls the glideslope indicator (this optical light source is called "meatball"), while image position and roll angle are determined by prism-controlled servos.

SERVOS COMMON TO CIG AND TIG OPERATIONS. Target Image Projection (TIP) servos that position the target (aircraft carrier, airplane, etc.) image within the dome are common to both TIG and CIG operations. Azimuth and elevation servos control position of the image with respect to the observer. A roll servo provides compensation for roll angle induced by combined azimuth/elevation commands.

SUMMARY OF SERVO SYSTEMS EVALUATED. The following is a summary of the visual system servos evaluated in this study:

a. Target Image Projection (In Dome)

(1) azimuth
(2) elevation
(3) roll

b. Fresnel Lens Optical Landing System (In Dome)

(1) pitch wedge (x position)
(2) pitch wedge (y position)
(3) roll
(4) meatball

c. Gantry Rate Servos

(1) x translation
(2) y translation
(3) z translation

d. Probe (In Gantry Mount)

(1) heading
(2) pitch
(3) roll
(4) command filter (shapes command signal to all probe servos)

As noted previously, the servo measurements taken for this report did not include an induced lag in the servo pre-filters.

## SERVO PERFORMANCE CRITERIA

This section describes the test procedures used and defines performance criteria for the frequency domain and time domain testing. Closed-loop servo performance is presented in the form of frequency domain and time domain data. In addition, static accuracy or repeatability of each servo system is presented for completeness.

FREQUENCY RESPONSE. A simplified block diagram of the servo system test setup is shown in Figure II-1. For frequency response tests, the servos were driven with sinusoidal signals generated by a Servomatic Analyzer. Test points, where data was recorded on an oscillograph strip recorder, are indicated in Figure II-1. Signals recorded included the drive (reference) signal, feedback signal, error signal, tachometer output, power amp drive and torque motor current.

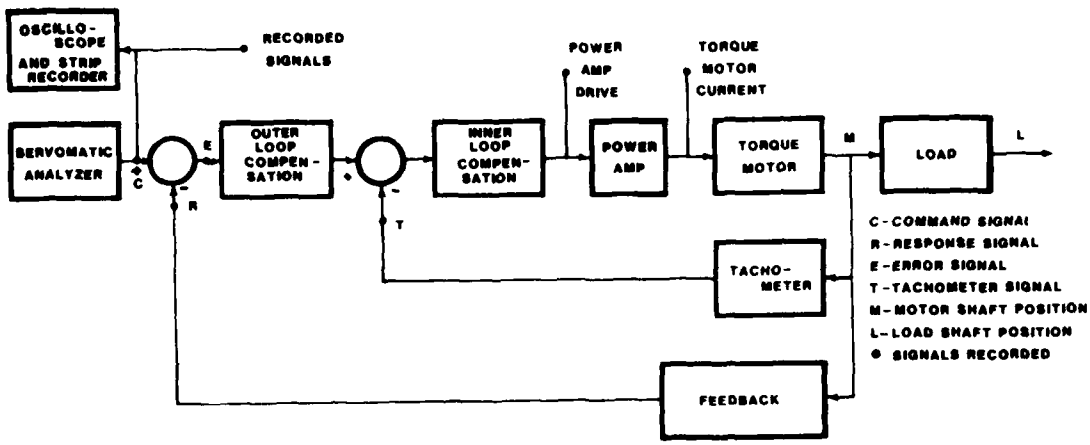


Figure II-1. Servo in Test Configuration

Basically there are two types of servos used in the Visual Technology Research Simulator (VTRS) lab: the non-continuous type with linear feedback potentiometers, and the continuous type with sine-cosine potentiometers or synchros (used in the probe servos only). The synchro uses the same principle as the sine-cosine potentiometer, except it is an alternating current device using transformer action. Figure II-2 illustrates the principle of the sine-cosine potentiometer for detection of servo error.

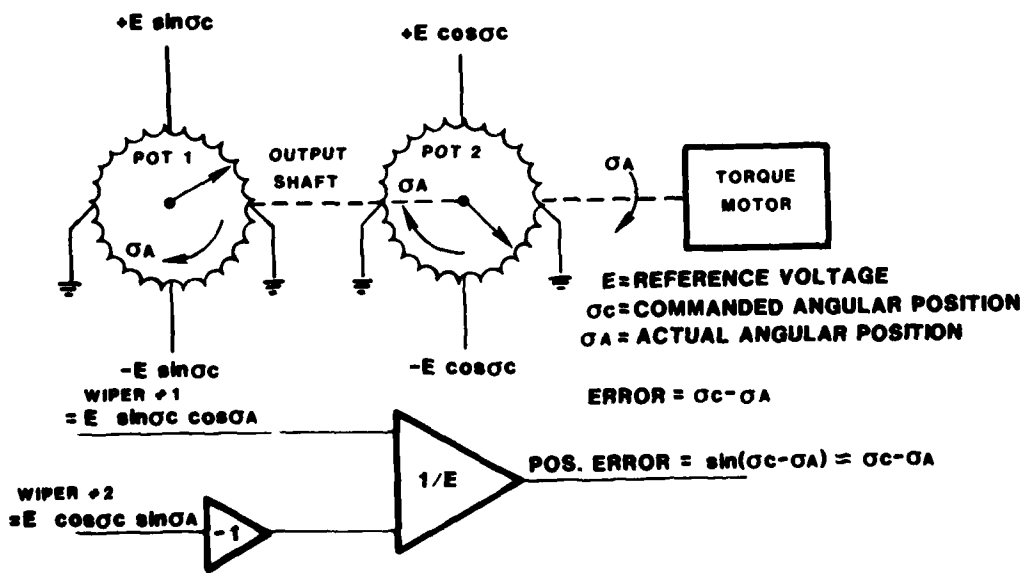


Figure II-2. Continuous Type Servos with Sin-Cos Potentiometer

For servos with non-continuous linear feedback potentiometers, closed loop frequency response was directly computed as the complex ratio of R/C (Figure II-1). However, the continuous servos with sine-cosine potentiometers (or synchros) do not have a feedback signal for direct derivation of closed loop performance.

Referring to Figure II-2, the sine-cosine device detects error directly from command and output shaft position. Thus, only command and error signals are available. Also, since two command signals are required, $\sin\theta_C$ and $\cos\theta_C$, special considerations were given to the signal drive technique.

Since all command signals were typically small (less than 10 degrees), $\sin\theta_C$ was approximated as $\theta_C$ and $\cos\theta_C$, as 1. Thus the servo can be driven by setting a fixed voltage = $\pm E$ across the cosine pot and then exciting the sine pot with a voltage = $\pm E \sin\theta_C$.

The continuous servo does not have a direct output or feedback signal, therefore closed loop frequency response must be determined from error response. Using the command and error signals, closed loop frequency response was determined as follows:

$$\text{Closed Loop Transfer Function} = R(j\omega)/C(j\omega)$$

$$= 1 - E(j\omega)/C(j\omega)$$

Where C = command complex amplitude

R = response complex amplitude

E = error complex amplitude

E/C can be expressed as $M(j\omega)e^{j\theta(j\omega)}$

Where M = magnitude ratio of E/C

$\theta$ = angle of E - angle of C

$$E/C = M(\cos\theta + j\sin\theta)$$

$$R/C = 1 - E/C$$

$$= 1 - M\cos\theta - jM\sin\theta$$

$$\text{Magnitude of } R/C = [(1-M\cos\theta)^2+M^2\sin\theta^2)]^{1/2}$$

$$\text{Phase Angle of } R/C = \tan^{-1} \frac{M\sin\theta}{M\cos\theta - 1}$$

Servo bandwidth is defined as that frequency associated with a closed loop magnitude ratio of -3 db (0.707).

At all drive frequencies, magnitude of the sinusoidal excitation was maintained at levels consistent with minimum distortion or saturation within the loop to stay in the linear region of operation. Armature current in the drive motor was also monitored to assure that torque saturation did not occur during testing.

STEP RESPONSE. All of the visual system servos were subjected to step commands to determine response time and stability characteristics. As was the case with frequency response, command levels were made as large as possible consistent with staying in the linear operating region.

Response time is defined in this report as that time associated with a response equal to 63 percent of the command. Damping ratio is estimated by approximation to a second-order system response, using overshoot as the primary indicator.

## VISUAL SERVO PERFORMANCE

The following visual servo performance data consists of closed loop frequency response, step response and static accuracy or repeatability. Criteria for measuring performance in both time and frequency domains was discussed above. Static repeatability was included since it measures not only low frequency servo performance, but also the capacity to properly align optical systems using the servo systems directly as the aiming device. Tabular data is summarized in Tables II-1-4. Response curves are given in Figures II-3 through II-14.

TIP SERVOS. The azimuth and elevation Target Image Projector (TIP) servos are non-continuous with linear potentiometers and are connected to the load by direct drive. Roll, however, is continuous with sine-cosine pots and is connected to the load through anti-backlash gears.

Frequency Response. Figures II-3 and II-4 present magnitude and phase shift for the closed loop frequency response of the TIP servos. Bandwidths of the TIP servo responses are presented in Figure II-3 and the tabulated data summarized in Table II-1.

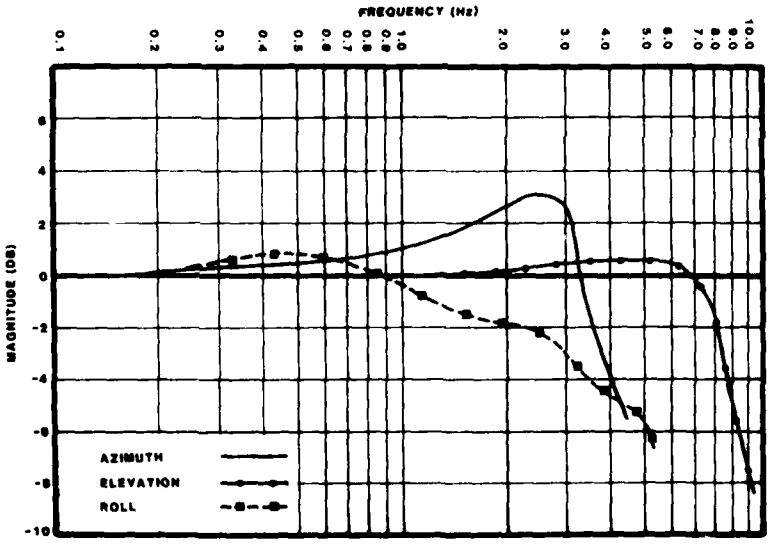


(Magnitude vs. Frequency)

Figure II-3. TIP Servos - Frequency Responses

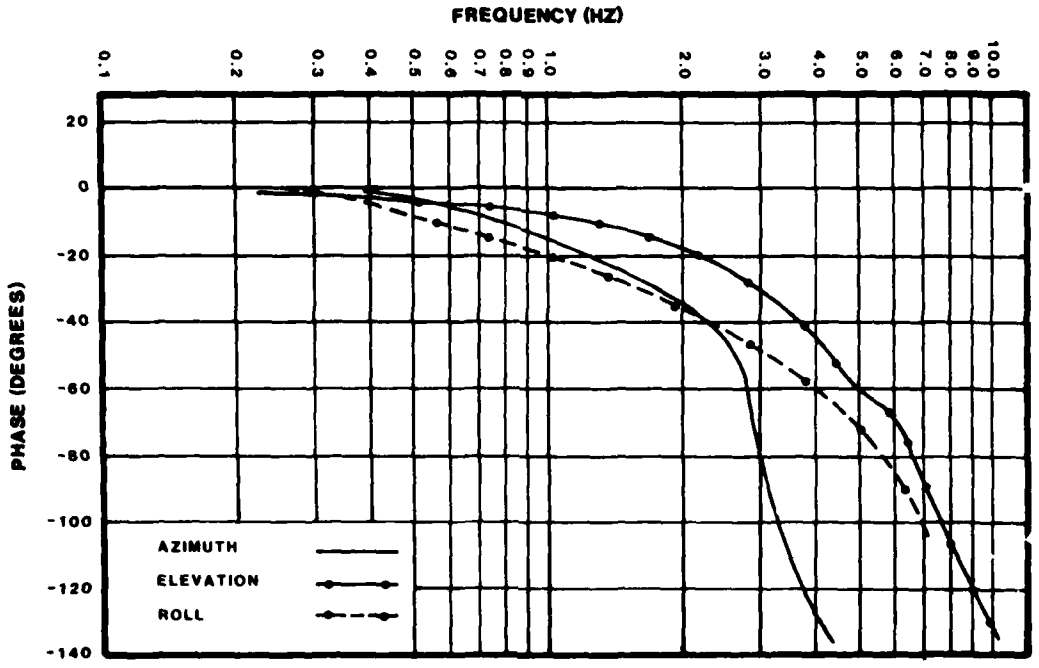


(Phase vs. Frequency)

Figure II-4. TIP Servos - Frequency Responses

TABLE II-1. VISUAL SERVOS PERFORMANCE SUMMARY - TIP

| | Bandwidth (1) (Hz) | Step Response | | Static Repeatability | Range Limits |
|---|---|---|---|---|---|
| | | Response Time (2) (msec) | Damping Ratio | | |
| AZ | 3.8 | 67 | 0.4 | ± 0.75 arc min | + 95°, -135° |
| EL | 8.5 | 43 | 0.5 | ± 0.8 arc min | + 65°, -55° |
| De Roll | 3.0 | 55 | CTO | ± 1.4 arc min | Cont |

NOTES:
1. -3 db point
2. 63 percent of Command Amplitude
3. (CTO) Critical to Overdamped
4. (Cont) Continuous

Step Response. For purpose of direct comparison, step responses for the TIP servos were normalized. From Figure II-5, the response times and "second-order" equivalent damping ratios are as tabulated in Table II-1.

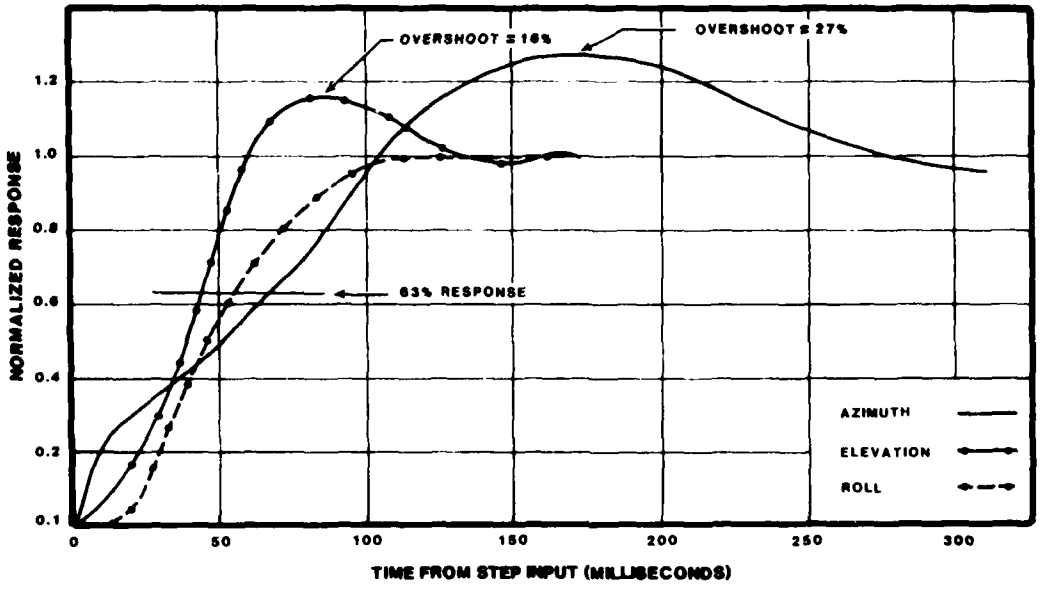


Figure II-5. Target Projector Servo Responses to Step Inputs

Static Repeatability. Static repeatability measurements were made on each servo unit. At selected operating points, the servo load was pushed away manually from its commanded position and then allowed to slowly return, each time recording the final static servo position. Worst case of static repeatability for the TIP servo is summarized in Table II-1.

FLOLS SERVOS. The pitch wedges, which control the position of the model image within the target projected field of view, are continuous-type servos with sine/cosine potentiometers. The wedge assemblies are driven through anti-backlash gears.

The roll servo is also a continuous-type of control with sine/cosine potentiometer. The roll prism is driven through an anti-backlash gear train.

The Fresnel Lens Optical Landing System (FLOLS) meatball is a non-continuous type servo with linear pot feedback. Meatball motion is rectilinear with the assembly driven through a Roh'lix gear (converts rotational motion to rectilinear motion).

Frequency Response. Closed loop magnitude ratio and phase plots of the FLOLS servo system are presented in Figures II-6 and II-7. The two pitch wedges, the FLOLS roll servo and meatball servo performance data are summarized and presented in Table II-2.

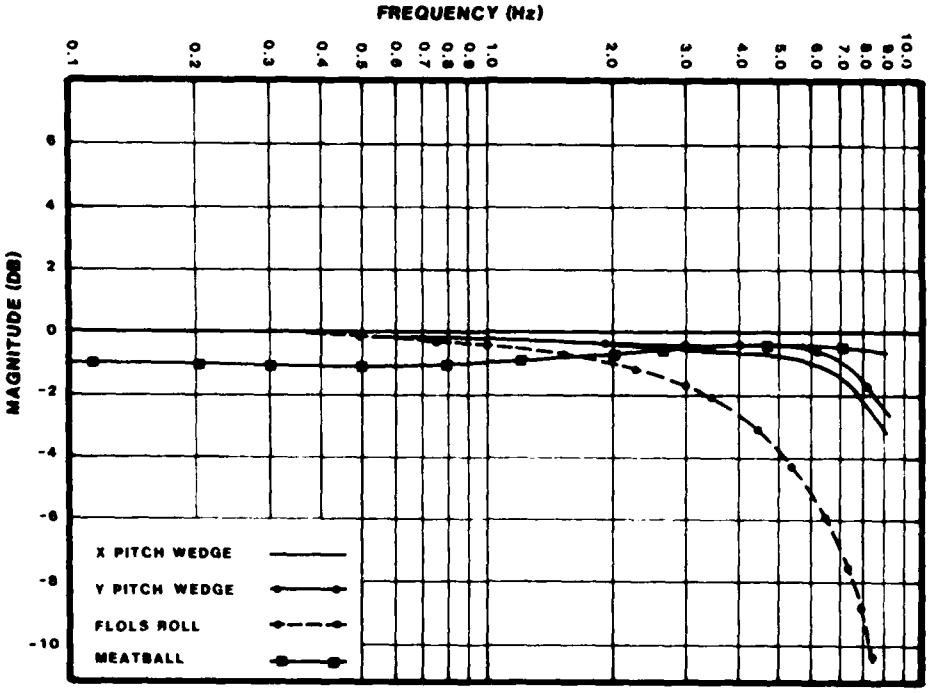


(Magnitude vs. Frequency)

Figure II-6. FLOLS Servos - Frequency Responses

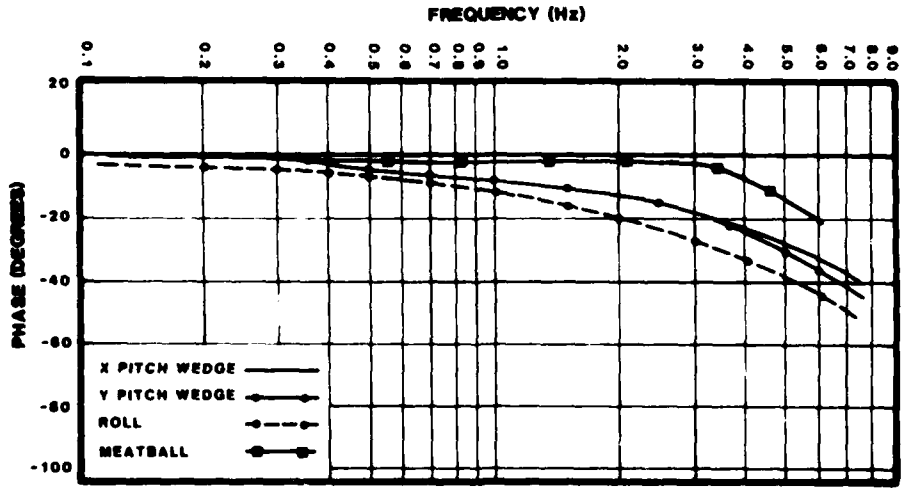


(Phase vs. Frequency)

Figure II-7. FLOLS Servos - Frequency Responses

TABLE II-2. VISUAL SERVOS PERFORMANCE SUMMARY - FLOLS

| | Bandwidth (1) (Hz) | Step Response | | Static Repeatability | Range Limits |
|---|---|---|---|---|---|
| | | Response Time (2) (msec) | Damping Ratio | | |
| X-PW | 9. | 28 | CTO (3) | ± 0.003 arc min | Cont (4) |
| Y-PW | 9. | 28 | 0.47 | ± 0.009 arc min | Cont |
| Roll | 4.2 | 42 | CTO | ± 0.003 arc min | Cont |
| Ball | 60 (5) | 7 | CTO | ± 0.002 ball width | ± 2 ball widths |

NOTES:
1. -3 db point
2. 63 percent of Command Amplitude
3. (CTO) Critical to Overdamped
4. (Cont) Continuous
5. Estimated From Step Response

Step Response. Normalized step responses of the FLOLS servo are presented in Figure II-8. Response times and damping ratios for the FLOLS servos are summarized in Table II-2.

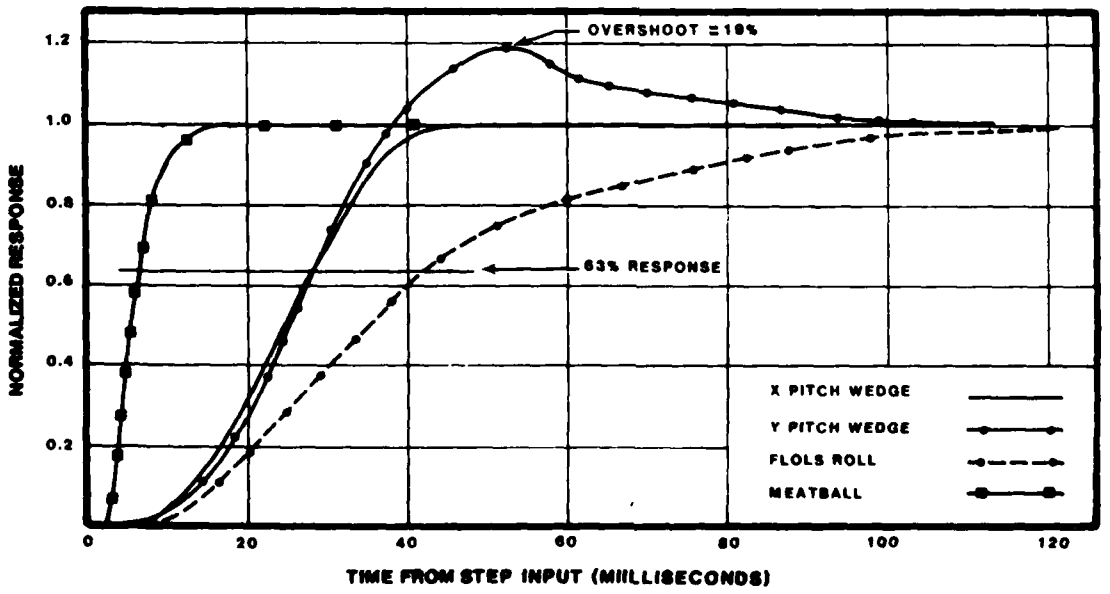


Figure II-8. FLOLS Servo Responses to Step Inputs

Static Repeatability. A summary of static repeatability performance for the FLOLS servos is presented in Table II-2.

GANTRY RATE SERVOS. The three gantry servos, x, y, and z translations, are rate commanded by the computer. The y and z translations are both driven through Roh'lix gear systems, while the x axis is controlled by driving a wheel along a guide rail, using friction between the wheel and rail to propel it. As discussed previously, the vidicon and associated optical systems are mounted on the z assembly which moves in and out of the vertically mounted model board. The z assembly is mounted on the y assembly which translates vertically. The y and z gantry assemblies are both mounted on the x assembly which provides longitudinal motion to the other two assemblies.

Closed loop performance data presented for the gantry servos measures translational rate response to translational rate command. All of the other servo system performance data presented is related to position (angular and translational) response.

The tachometer outputs were used as the basic output signal, although a rectilinear potentiometer was mounted on each axis to record and correlate position with rate data derived from the tachometer.

Frequency Response. Frequency response data for the closed loop gantry rate servos is presented in Figures II-9 and II-10. As expected, bandwidths of the three gantry rate servos vary according to the inertial load being driven. The gantry rate servo performance is summarized in Table II-3.

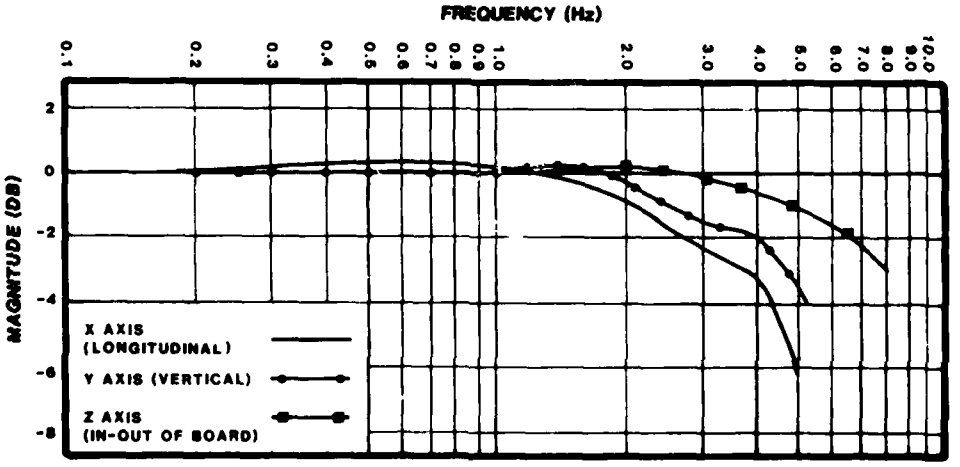


(Magnitude vs. Frequency)

Figure II-9. GANTRY Rate Servos - Frequency Responses

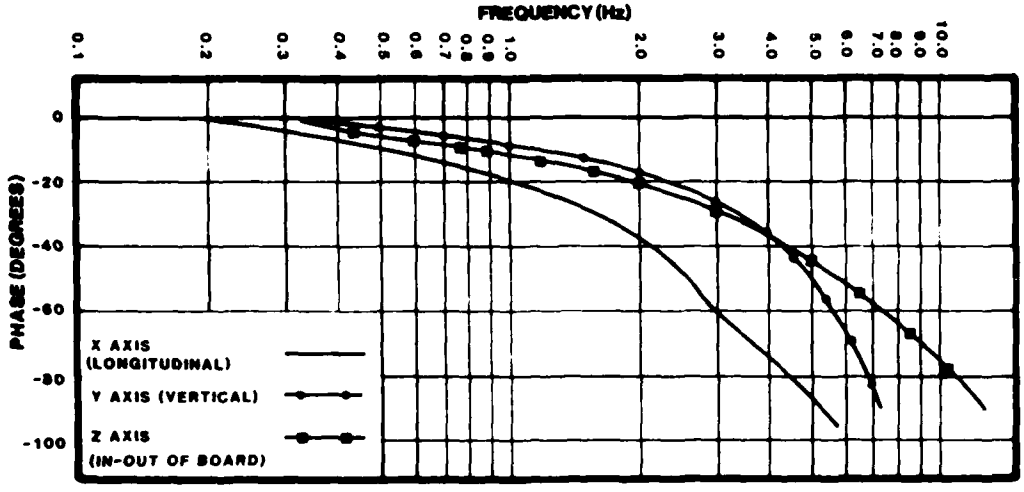


(Phase vs. Frequency)

Figure II-10. GANTRY Rate Servos - Frequency Responses

TABLE II-3. VISUAL SERVOS PERFORMANCE SUMMARY - GANTRY

| | Bandwidth (1) (Hz) | Step Response | | Static Repeatability | Range Limits |
|---|---|---|---|---|---|
| | | Response Time (2) (msec) | Damping Ratio | | |
| X axis | 3.8 | 74 | CTO | (4) | ± 11 ft. |
| Y axis | 4.7 | 36 | CTO | (4) | ± 11 ft. |
| Z axis | 8.0 | 30 | CTO | (4) | ± 2.7 ft. |

NOTES:

1. -3 db point
2. 63 percent of Command Amplitude
3. (CTO) Critical to Overdamped
4. This data is not defined for this system

Step Response. Step rate commands were issued to each of the gantry axes. Normalized responses to these rate commands are presented in Figure II-11. Response times and damping ratios for the gantry system are presented in Table II-3.

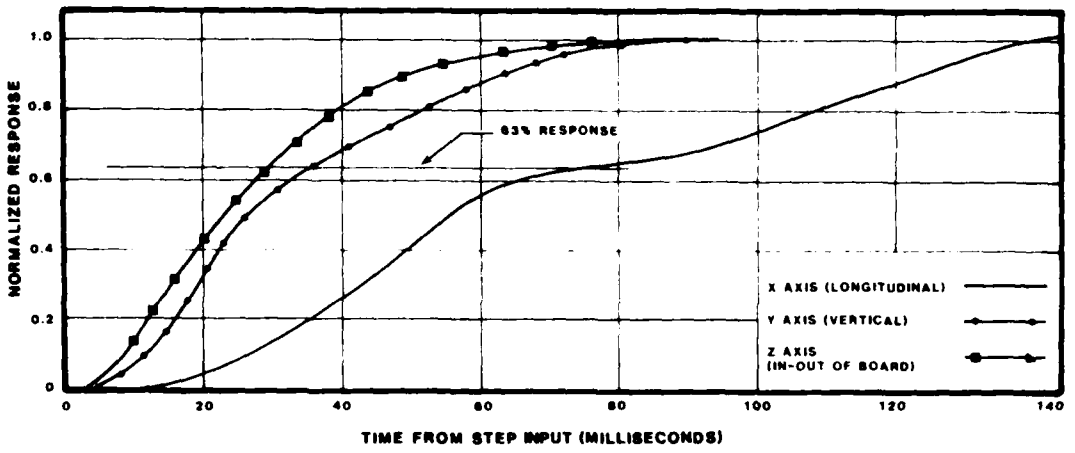


Figure II-11. GANTRY Servo Responses to Step Rate Inputs

Static Repeatability. Static repeatability is not presented for the gantry rate servos since they are rate systems and static repeatability is not defined for those systems. As discussed earlier, the position control loop is closed in software and position accuracy will be determined through software tests.

PROBE SERVO. The probe servos, heading, pitch and roll, all have synchros as error sensors. These synchros are connected to the optical load through anti-backlash gears. A command pre-filter is in cascade with each of the probe servos. This filter is slow compared to the probe servos, and tends to dominate the overall response characteristic. The command pre-filter response is, however, still very fast and meets system requirements.

Frequency Response. Closed loop frequency responses of the probe servos are presented in Figures II-12 and II-13. Performance data for these servos is summarized in Table II-4.

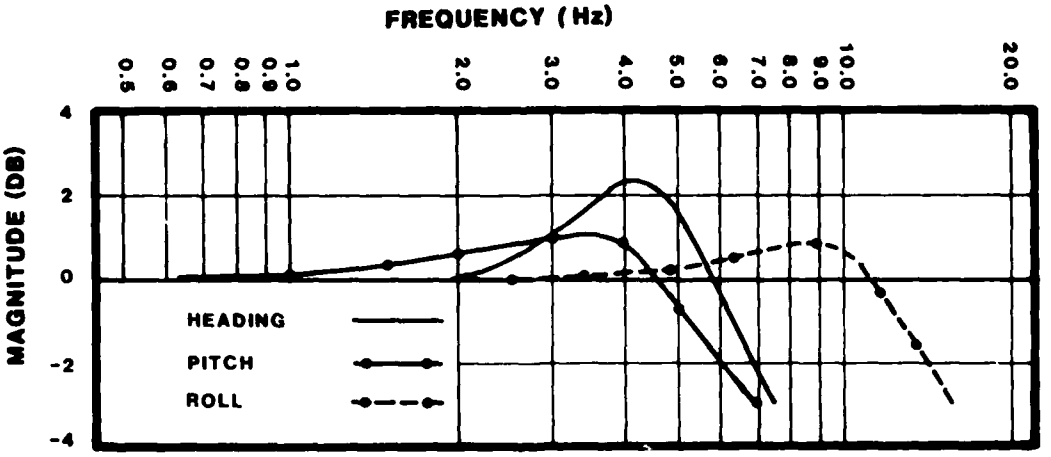


(Magnitude vs. Frequency)

Figure II-12. PROBE Servos - Frequency Responses

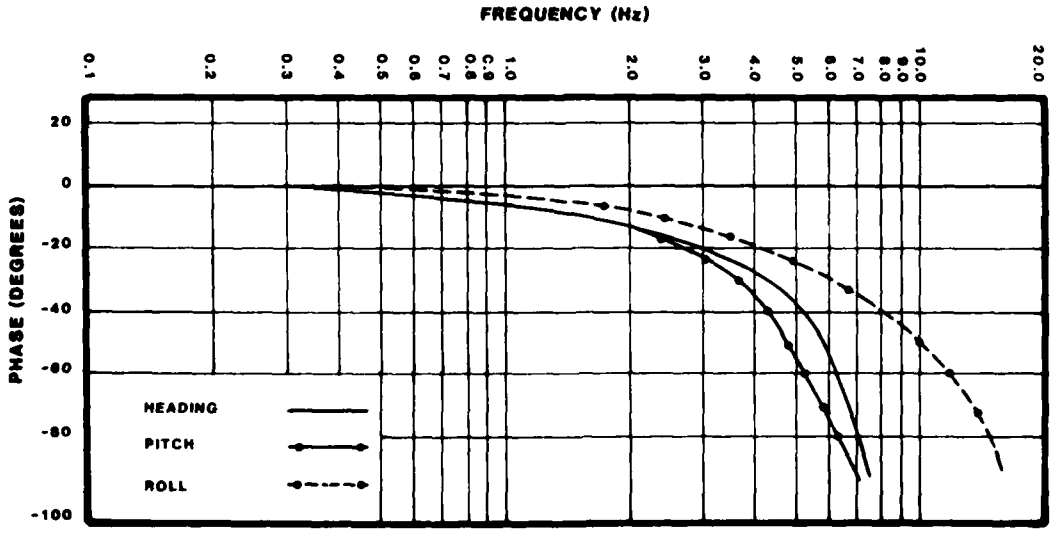


(Phase vs. Frequency)

Figure II-13. PROBE Servos - Frequency Responses

TABLE II-4. VISUAL SERVOS PERFORMANCE SUMMARY - PROBE

| | Bandwidth (1) (Hz) | Step Response | | Static Repeatability | Range Limits |
|---|---|---|---|---|---|
| | | Response (2) Time (msec) | Damping Ratio | | |
| Heading | 7.5 | 31 | 0.56 | ± 0.15 arc min | Cont |
| Pitch | 7.0 | 34 | 0.43 | ± 0.075 arc min | + 45°, -135° |
| Roll | 15.1 | 17 | 0.46 | ± 0.075 arc min | Cont |
| Pre-Filter | (3) | 60 | 0.74 | (3) | (3) |

NOTES:
1. -3 db point
2. 63 percent of Command Amplitude
3. Information not applicable to pre-filter data

Step Responses. Normalized step responses for the probe servos are presented in Figure II-14. The command pre-filter, which is cascaded with each of the probe servos, has a significantly slower response time of 60 msec and thus dominates the response. Response time and damping ratios are summarized in Table II-4.

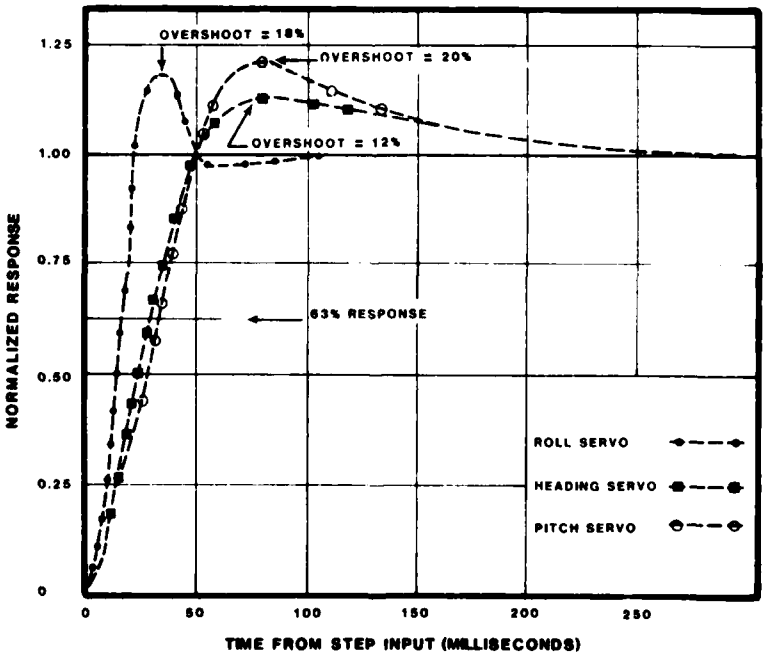


Figure II-14. PROBE Servos Responses to Step Inputs

Static Repeatability. Static repeatability test results for the probe servos are presented in Table II-4.

# SECTION III

# THE MOTION SYSTEM

## MOTION PLATFORM DESCRIPTION AND OPERATING LIMITATIONS

Motion in the VTRS/CTOL mode is provided by a six-degree-of-freedom synergistic system utilizing six 48 inch stroke hydraulic actuators (legs). Motion provided by the system simulates activity about all aircraft axes. Platform motion signals are generated by the manipulation of cockpit controls (Linkage as discussed in Section I) through computer functions to the main hydraulic distribution manifold (Figure III-1), then to the appropriate actuator for system response. Platform motion responses are particularly sensitive to signal influences such as would be provided by catapult launches, arrested landings, stall buffets, rougn air and other maneuvers associated with induced acceleration ("G") forces.

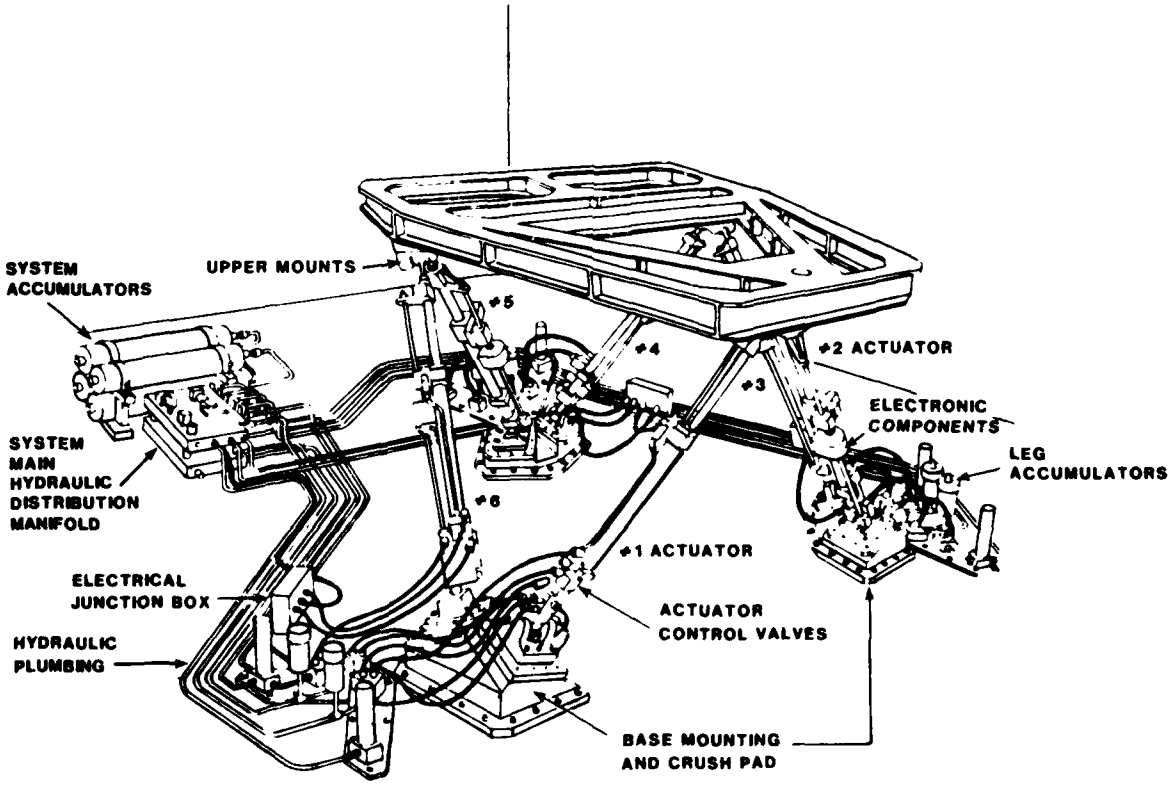


Figure III-1. VTRS Motion Platform Depicting Hydraulic Actuators and Fluid Distribution System

Cockpit configuration represents the T2C aircraft, which has been in fleet training service for more than a decade and has been the intermediate jet training vehicle for the majority of today's active duty Navy and Marine Corps pilots.

Platform operating limitations are depicted in Table III-1. Acceleration measurements listed in Table III-1 were taken utilizing a 15,000 lb. load factor and a displacement of each degree of freedom operation from the normal or neutral position.

TABLE III-1. PLATFORM OPERATING LIMITATIONS

| | SPECIFIED | | | MEASURED |
|---|---|---|---|---|
| | DISPL | VEL | ACCEL | ACCEL |
| Pitch | +26°<br>-24° | ±15°/sec | ±60°/sec$^2$ | ±145°/sec$^2$ |
| Roll | ±22° | ±15°/sec | ±170°/sec$^2$ | ±233°/sec$^2$ |
| Yaw | ±29° | ±15°/sec$^2$ | ±60°/sec$^2$ | ±233°/sec$^2$ |
| Vertical | +23<br>-32 | ±24"/sec | ±.8G | ±.8G |
| Longitude | ±48"/Fwd<br>Aft | ±24"/sec | ±.8G | ±.8G |
| Lateral | ±42" left/<br>right | ±24"/sec | ±.6G | ±.8G |

MOTION SYSTEM SOFTWARE

The motion platform software accepts inputs of aircraft acceleration, velocity and position. It transforms and filters them into six motion drive commands: roll, pitch, yaw, longitudinal, lateral and vertical. The platform position commands are geometrically transformed into leg position commands required to achieve the desired platform position. The platform, in the process of achieving the commanded position, undergoes velocity changes which create the desired onset and gravity align acceleration cues.

SYSTEM SOFTWARE. The platform system software parameter flow is summarized in Figure III-2.

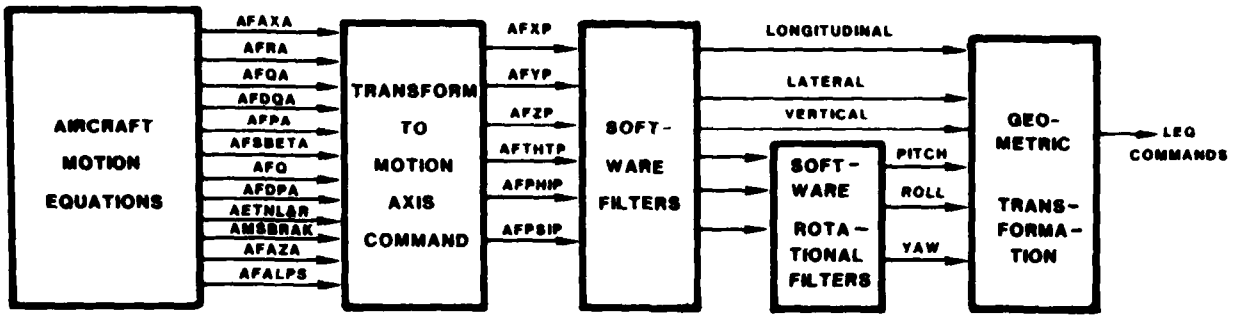


Figure III-2. Motion Parameter Flow

Aircraft Drives.

Pitch. Pitch position is driven by the following aircraft flight parameters:

a. Aircraft pitch acceleration - This parameter generates a positive onset cue acceleration and negative acceleration for velocity washout. It is characterized by a high frequency response.

b. Aircraft pitch velocity - This parameter also generates an acceleration cue and washout which is added to the term in a. However, since it is the integral of acceleration, the accelerations generated are slower and longer in duration, creating an overall "slower and longer" cue and washout. This drive has the advantage of providing position washout as aircraft velocity goes to zero.

c. Aircraft yaw rate squared - This is the "$W^2R$" centrifugal acceleration term that exists during a yaw and is manifested in a longitudinal acceleration. It is simulated by a pitch position command producing a gravity align.

d. Aircraft angle of attack - Platform pitch attitude is commanded as a function of angle of attack to simulate the low frequency component of aircraft pitch attitude. Using angle of attack instead of aircraft pitch provides scaled limiting during conditions of excessive pitch.

e. Aircraft longitudinal acceleration - This parameter drives the gravity align term by generating a platform pitch position component which produces a gravity align term. The resultant platform steady state response produces a gravity vector variation that depends on the attitude of the platform. The pitch software performs two basic functions: 1) provides a pitch acceleration cue response by developing a rate of change of platform position which generates the onset component; and 2) provides a simulation of aircraft longitudinal acceleration by generating a platform steady state position which is a scaled equivalent of longitudinal acceleration.

The onset cue filter passes the high frequencies and rejects the low, while the gravity align filter passes the low frequencies and rejects the high frequencies. This is a reasonable approach since the gravity align is using pitch position to simulate longitudinal acceleration. For slowly-changing longitudinal accelerations, this method is deceptive enough to be acceptable; but for fast accelerations, rapid pitch changes and oscillations responding to longitudinal accelerations may become false cues. Therefore, if the high frequency accelerations are filtered by the gravity align, only the frequencies low enough to be acceptable for gravity align will be present.

f. AFTHTP - The platform pitch position command, AFTHTP, is a function of the variables presented below. The software flow diagram for pitch is shown in Figure III-3. Axial acceleration due to pitch velocity squared is considered negligible and hence is not included. Computer generated step responses of the software are shown in Figures III-4, III-5, and III-6.

AFTHTP = f(AFAXA, AFQA, AFDQA, AFALPS, AFRA)

where

AFAXA = aircraft body axis longitudinal acceleration

AFQA - aircraft body-axis pitch rate

AFDQA - aircraft body axis pitch acceleration

AFALPS - aircraft angle of attack (modified to incorporate stall effects)

AFRA - body axis yaw rate

AFMAXLG - lag term to slow response of gravity align term

AFMTHLG - provides scaling and velocity washout for pitch command

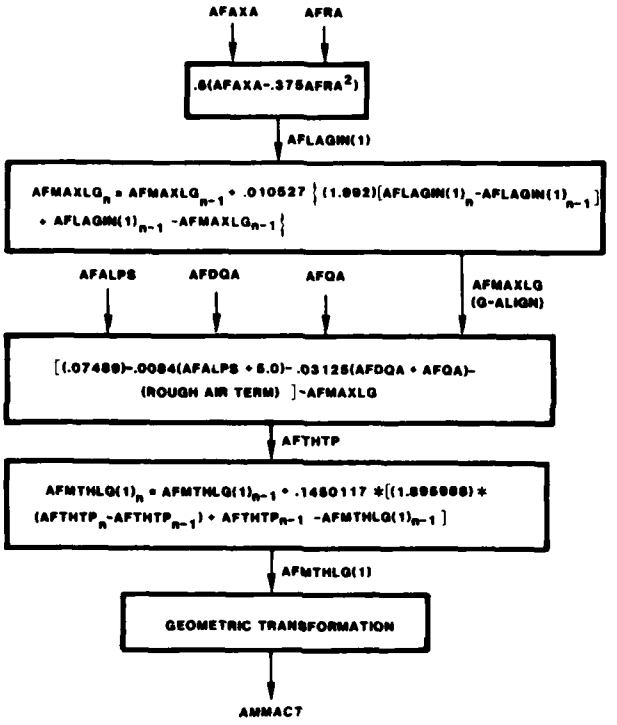


Figure III-3. Platform Pitch Software

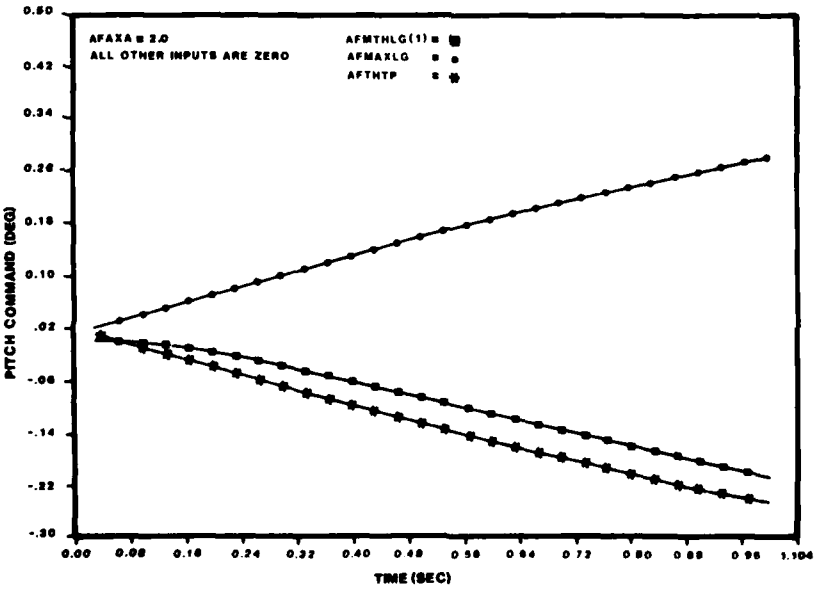


Figure III-4. Pitch Gravity Align Due to Aircraft Longitudinal Acceleration Step Input

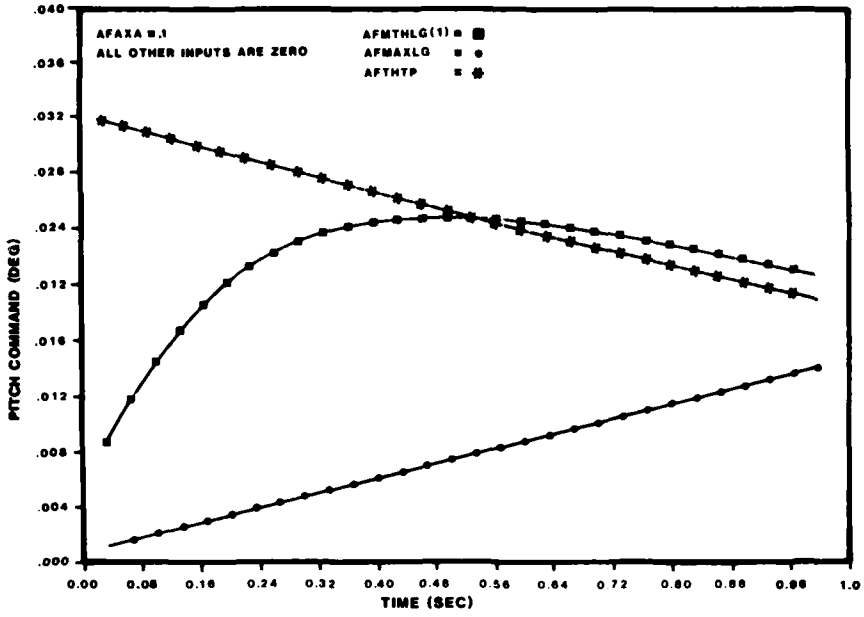


Figure III-5. Pitch Gravity Align Due to Aircraft Longitudinal Acceleration Step Input

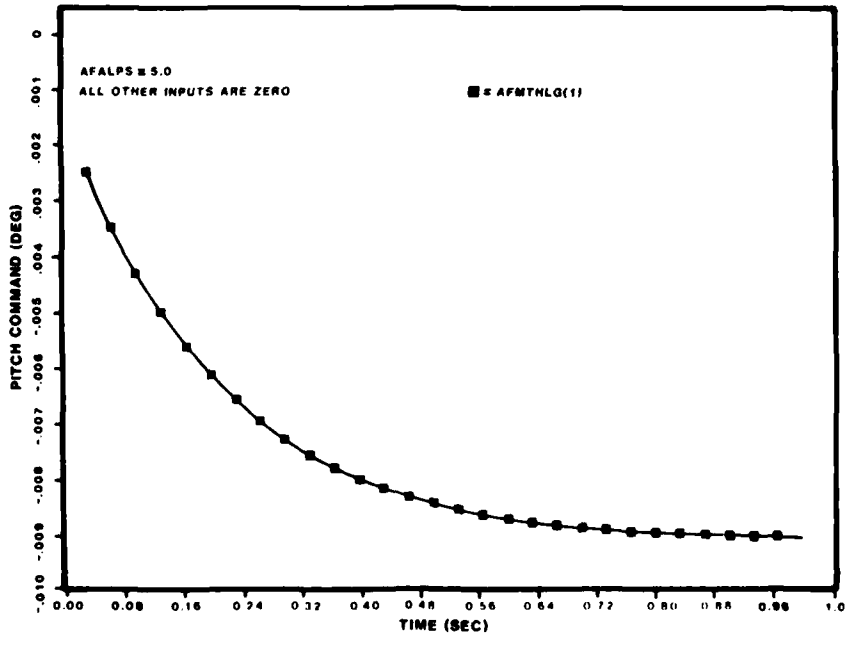


Figure III-6. Pitch Onset Due to Aircraft Angle of Attack Step Input

Roll. Platform roll is driven by aircraft roll rate and roll acceleration. Roll gravity align is provided as a function of AFSBETA (sideslip angle) and aircraft velocity (dynamic pressure). Sideslip angle is a measure of the forces encountered in an uncoordinated turn and is simulated by a steady state platform roll output. The roll flow diagram is shown in Figure III-7. A typical software filter response to aircraft roll rate step input is shown in Figure III-8. Note, that using roll rate instead of roll acceleration, as the drive decreases lead and passes lower frequencies, this increases the duration of the acceleration pulse (cue time) with, however, some increase in lag time. The AFAYA force due to bank angle is not included as a correction. The platform roll command, AFPHIP, is a function of the following:

$$AFPHIP = f(AFPA, AFQ, AFSBETA, AFDPA)$$

where

AFPHIP - roll platform command

AFPA - aircraft body axis roll rate

AFQ - dynamic pressure

AFSBETA - sine of aircraft sideslip angle

AFDPA - aircraft body axis roll acceleration

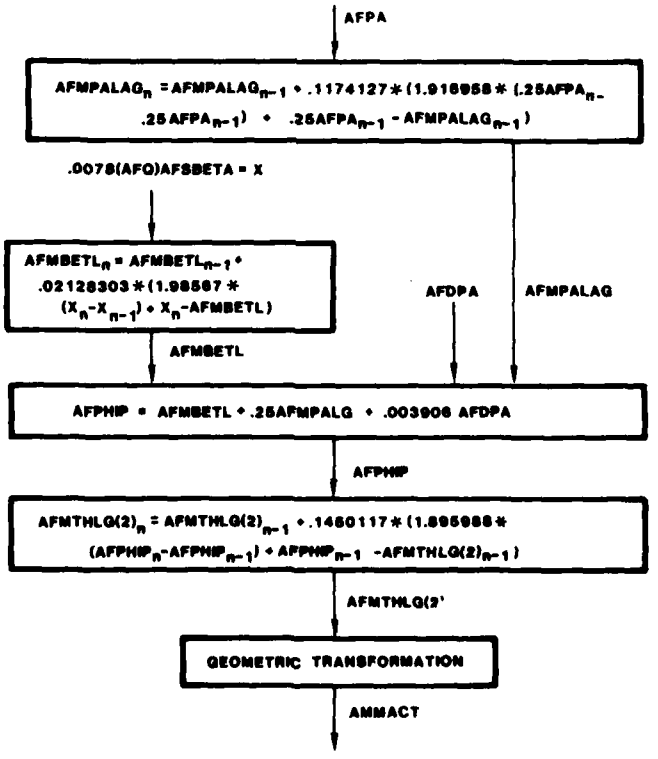


Figure III-7. Platform Roll Software

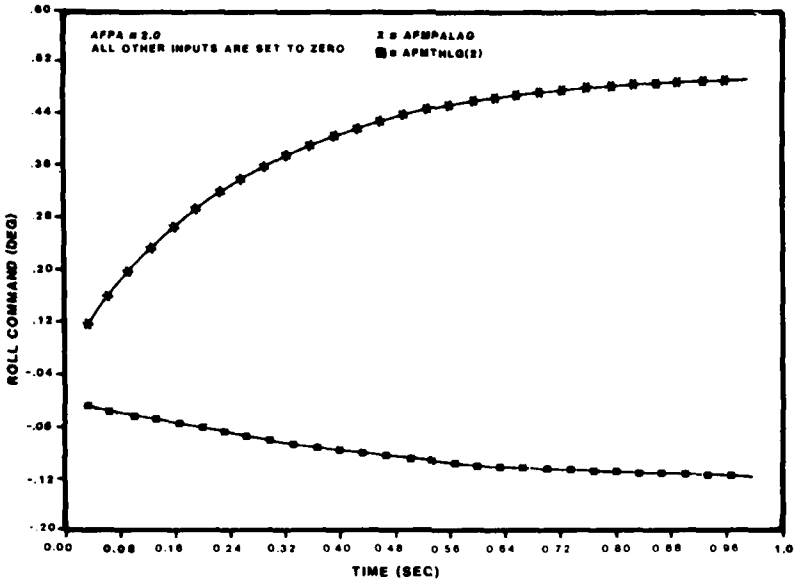


Figure III-8. Roll Onset Due to Aircraft Roll Rate Step Input

Yaw. Yaw platform command (AFPSIP) is a scaled function of AFSBETA and is illustrated in the flow chart of Figure III-9. A typical software yaw filter response is shown in Figure III-10.

$$AFPSIP = f(AFSBETA)$$

where

AFSBETA - sine of aircraft sideslip angle

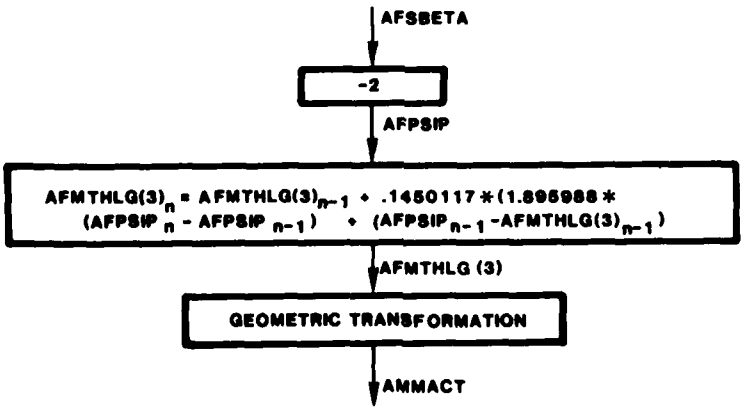


Figure III-9. Platform Yaw Software

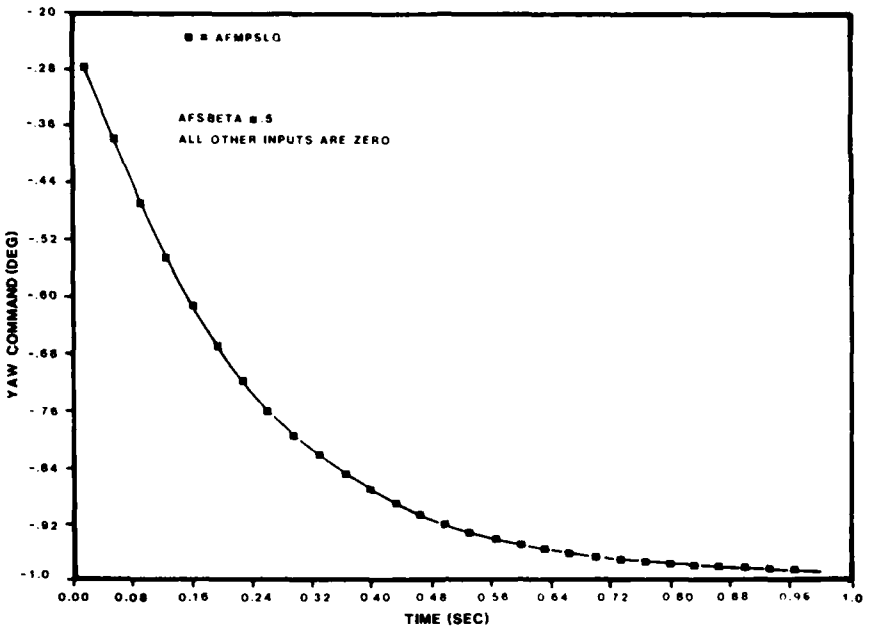


Figure III-10. Yaw Onset Due to Aircraft Sideslip Angle Step Input

Longitudinal Translation. The X or longitudinal platform position is a function of AFAXA and provides the longitudinal onset cues. It does not, however, include AFAXA components generated by pitch. The equation for AFXP is given below with the flow diagram presented in Figure III-11.

AFXP = f(AFAXA, AETNL, AETNR, AFHGR, AMSBRAKE, AFQ, AFXMCAT, AFFHOOK, AFMWASH)

where

AFMWASH - washout term for arrested landing

AFXP - longitudinal motion platform command

AFAXA - longitudinal aerodynamic acceleration

AETNL and AETNR - left and right aircraft engine rpm

AFHGR - ground reaction distance

AMSBRAK - speed brake deflection

AFQ - dynamic pressure

AFXMCAT - cat launch force

AFFHOOK - hook force

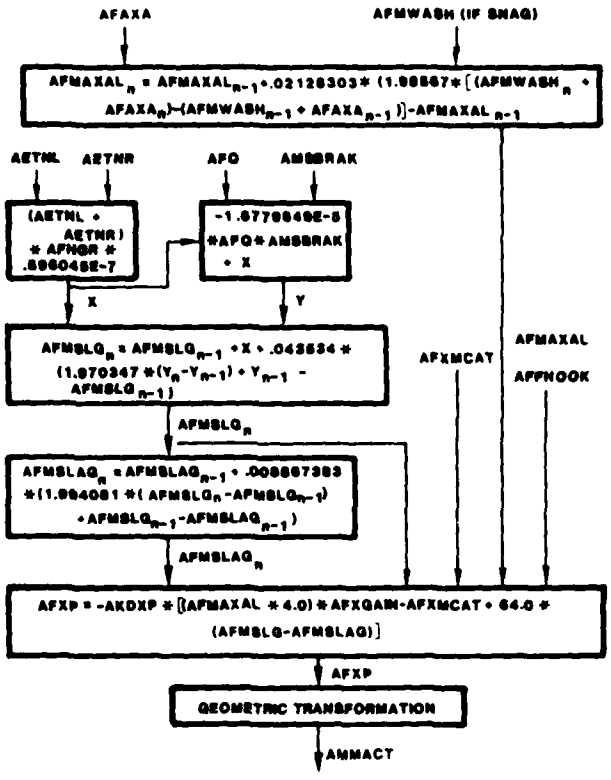


Figure III-11. Platform Longitudinal Software

The software filter response for a selected input value of AFAXA is shown in Figure III-12.

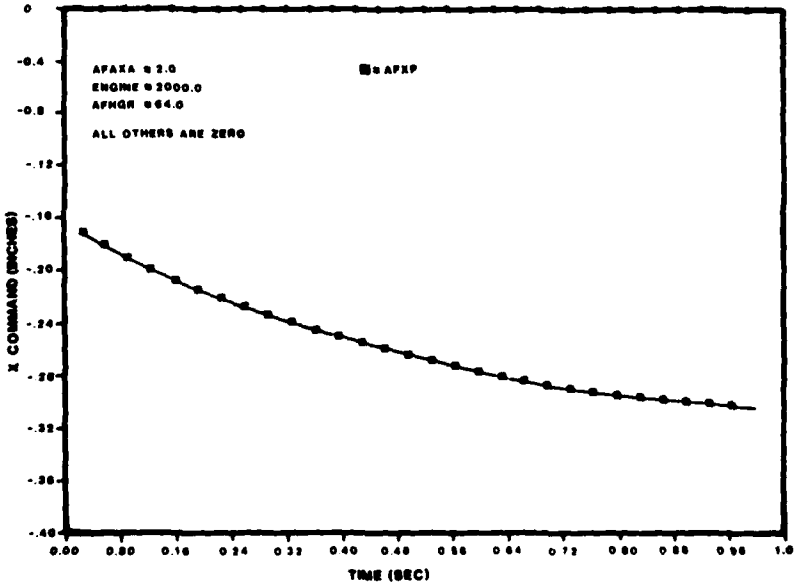


Figure III-12. Longitudinal Onset Due to Aircraft X-Axis Step Inputs

Lateral Motion Drive. Lateral motion drive is a function of AFPHIP, which is a function of roll rate, dynamic pressure, roll acceleration, sideslip, and yaw rate. The lateral acceleration is mainly a function of sideforce, which is largely dependent on BETA. Note that AFAYA is not used directly. The roll rate and yaw rate terms are corrections for displacement in the lateral direction resulting from roll and yaw. The form of the software is as follows and the flow chart is shown in Figure III-13.

AFYP = f(AFPHIP, AFRA)

where

AFPHIP = f(AFPA, AFQ, AFSBETA, AFDPA)

AFYP = lateral motion platform command

AFPA - aircraft body axis roll rate

AFDPA - aircraft body axis roll acceleration

AFRA - aircraft body axis yaw rate

AFSBETA - sine of aircraft sideslip angle

AFQ - dynamic pressure

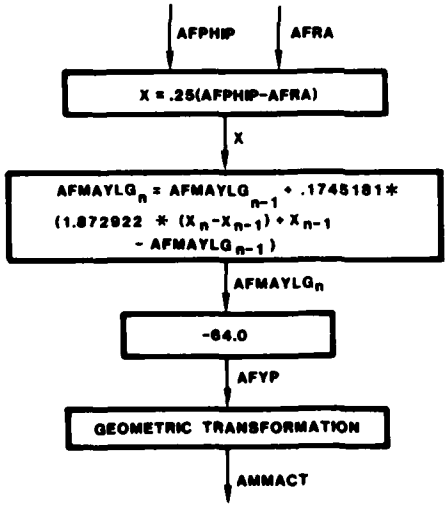


Figure III-13. Platform Lateral Software

A typical response for a selected value of input yaw rate is presented in Figure III-14.

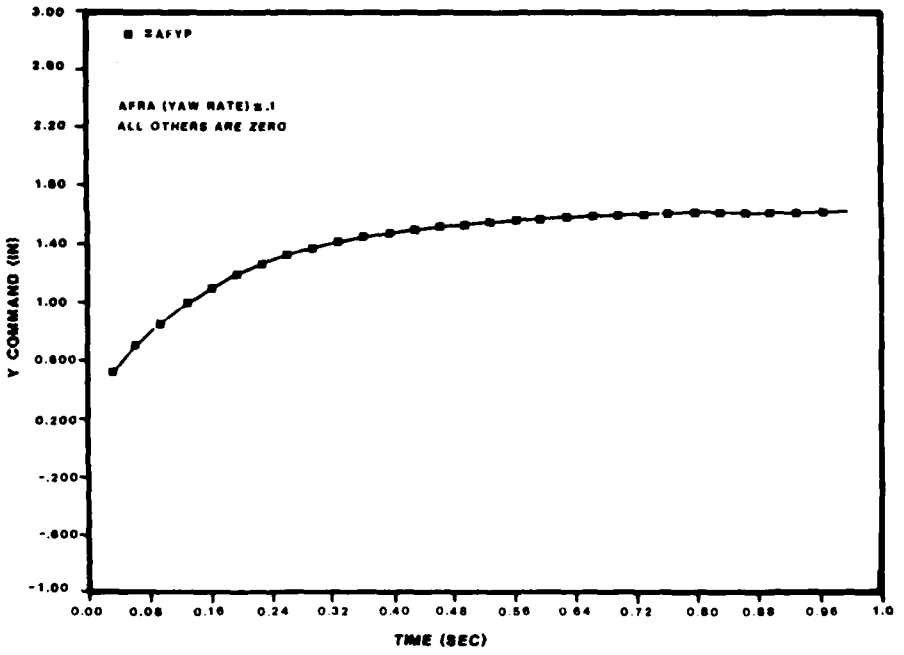


Figure III-14. Lateral Onset Due to Aircraft Yaw Rate

Vertical Motion Drive. The Z or vertical platform command provides an onset cue for aircraft vertical acceleration. This drive has a one-G correction for gravity but neglects the correction for Z due to aircraft pitch. This onset cue for acceleration is a function of:

AFZP = f(AFAZA, AFWRA, AFVCAL)

AFAZP - vertical motion platform drive

AFWRA - vertical rough air

AFAZA - vertical aircraft acceleration

AFVCAL - calibrated airspeed

AFMBPWO - G-break bump washout

The software flow is shown in Figure III-15 and typical responses are shown in Figure III-16.

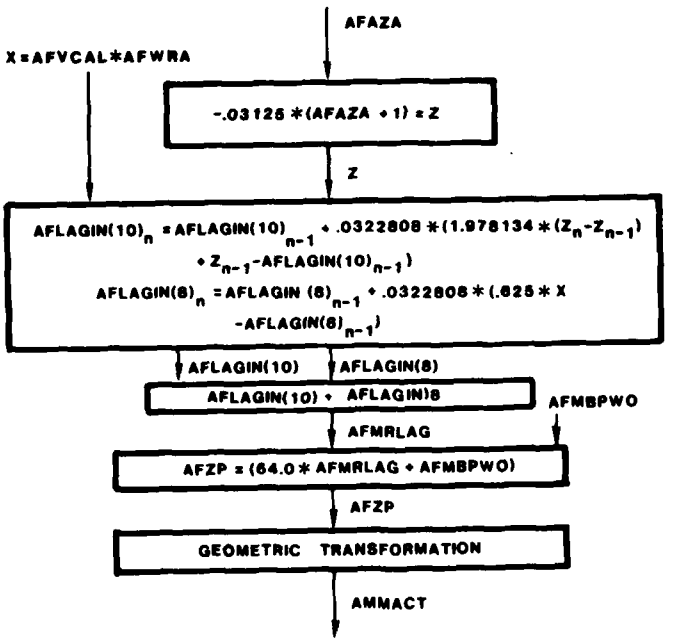


Figure III-15. Platform Vertical Software

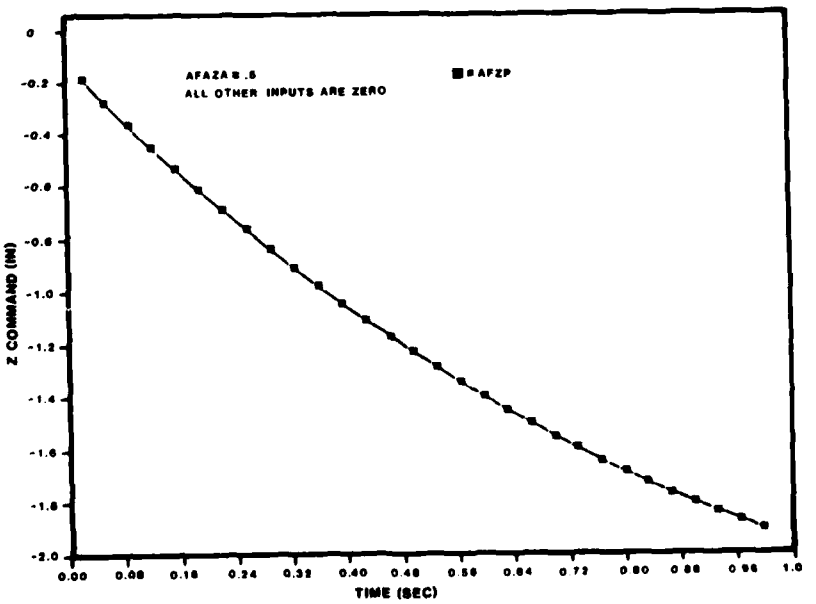


Figure III-16. Vertical Onset Due to Aircraft Z-Axis Step Input

## GENERATION OF ACCELERATION CUES

Detailed technical and algorithm information concerning the process of acceleration cue generation is contained in Appendix A.

## MOTION PLATFORM PERFORMANCE

The system performance was compared in heave step response with command through the existing 0.35 Hz leg hardware filters and through the maintenance filters (1.59 Hz). Platform acceleration magnitudes, rise times, durations, and washout magnitude were recorded and compared. Plots of these parameters are shown in Figures III-17 and III-18.

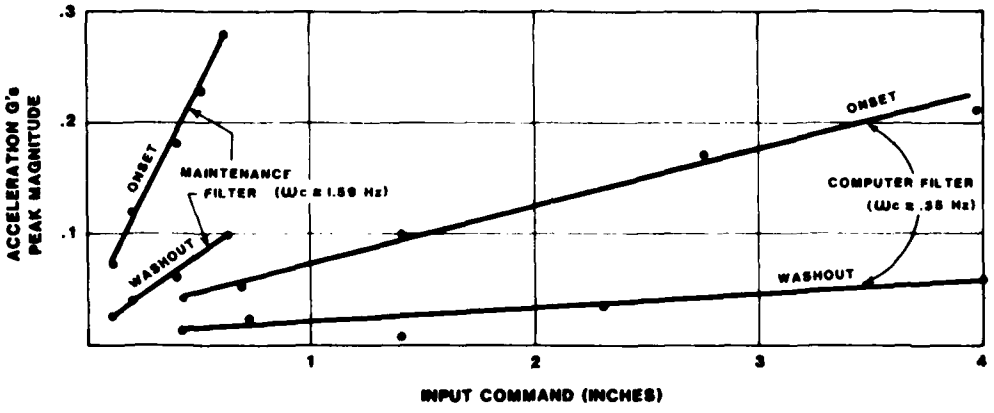


Figure III-17. Effect of Increased Filter Bandwidth of Onset Cuing Characteristics

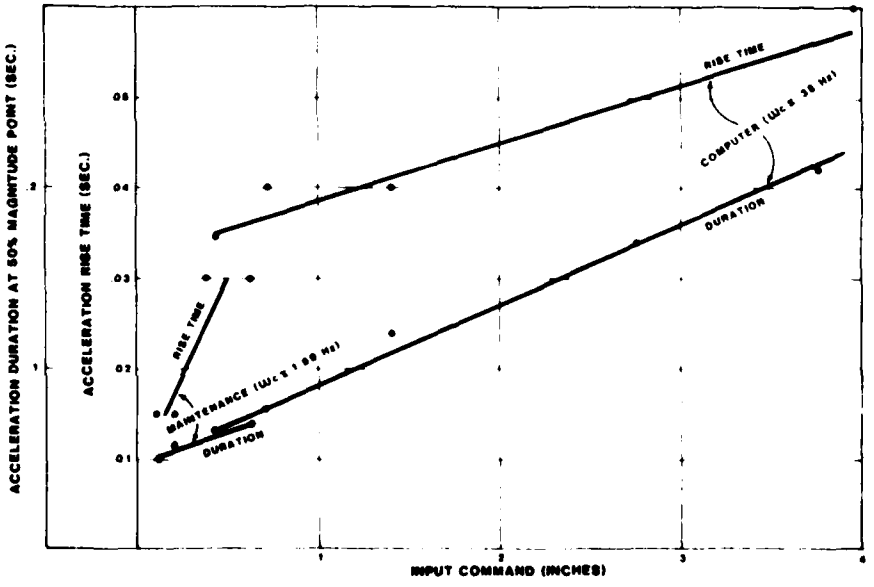


Figure III-18. Effect of Increased Filter Bandwidth of Onset Cuing Characteristics

The duration of the acceleration onset at an average 50 percent magnitude point is considerably longer for the 0.35 Hz filter than the 1.59 Hz filter, requiring a command of 3.9 inches for the acceleration cue duration threshold of 0.2 seconds to be reached. The 1.59 Hz filter achieved a pulse duration of 0.06 seconds at 1/2 inch of motion and 0.2 G's magnitude. The 50 percent acceleration duration for the 1.59 Hz filter per unit command change throughout a 0 to 1 inch command variation is small and stays around 0.05 sec whereas the 0.35 Hz filter acceleration duration increases at 0.09 sec/inch or 1.8 sec/G.

The slope of the 1.59 Hz filter curve of acceleration peak magnitude to command input is 0.4 G/inch whereas the 0.35 Hz is 0.05 G/inch. Observe that the higher 1.59 Hz pass filter results in much larger peak acceleration for smaller command inputs than the 0.35 Hz filter. The acceleration magnitude increases approximately linearly with command inputs. The 0.35 Hz filter increases at a considerably smaller rate than the 1.59 Hz filter.

The rise time difference for a command in the area of 1/2 inch is approximately 0.005 sec higher for the 0.35 Hz filter.

In general, it may be stated that increasing the filter cutoff to 1.59 Hz decreases the rise time of acceleration cues at low (under 1/2 inch) position input levels. The duration of the acceleration pulse decreases significantly and magnitude of the onset increases significantly. The washout magnitude increases significantly and duration of washout decreases. The pulse duration decreases to a 0.05 sec level approaching initiation of washout during a single iteration creating plus and minus pulses. This is well beyond the typical aircraft drive frequencies. The responses must be slower so that the lower (1 Hz) aircraft control input and aircraft response frequencies may be tracked without initiation of washout until sufficient cue time is attained. Sufficient smoothing of the iteration rate stepping must be provided by expanding the acceleration pulse and delaying washout response or essentially trading off acceleration magnitude for pulse duration. The data shows that even for a 1.59 Hz filter the acceleration cue and washout levels get very large. This, in itself, may not necessarily be undesirable, since high G cues with little delay are desirable; however, when coupled with the low pulse duration (cue time 0.2 sec required) and high washout magnitudes (less than 0.08G required), the response is unusable as a motion cuing system.

A filter in the area of 1.59 Hz could be used if coupled with the appropriate software gain and delay shaping modification, but the required effect would be to counteract the increase in bandwidth.

The software gain could be increased for more G's per unit command with minimal increase in rise time.

The G-align response is 0.6 sec and could be improved considerably; however, such a requirement has not been established.

Appendix A provides more detailed discussion and results of the motion cue measurement conducted during these tests.

# SECTION IV

# THE "G"-SEAT SYSTEM

The G-seat contains 29 controllable air bellows elements located in the seatpan, back rest, and thigh area, plus a lap belt. The system is open loop controlled and is designed to provide sustained acceleration cues only. A G-seat test system was constructed and utilized to evaluate G-seat performance as installed in the simulator. An 18 lb. load was placed on the seatpan and a linear potentiometer was mounted and attached to provide a reading of position displacement. The input signal was analog and applied at the motion cabinet input to the conflow control valve.

A static calibration of input pressure vs. bellows excursion was run on seatpan cell No. 10 with an 18 lb. load and is shown in Figure IV-1. The curve shows the response to be linear in the range of ±1 inch from midpoint between 3 and 8 PSI and saturating rapidly at points outside this range.

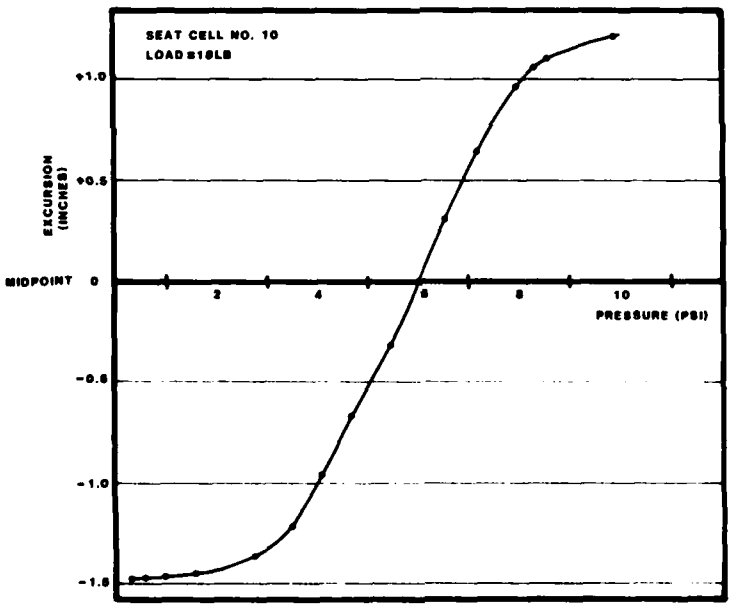


Figure IV-1. Cell Calibration Curve

A frequency response was run on this same cell (No. 10) with the 18 lb. load. The results are shown in Figure IV-2. The cell cutoff frequency (-3 db point) was at approximately 1.9 Hz.

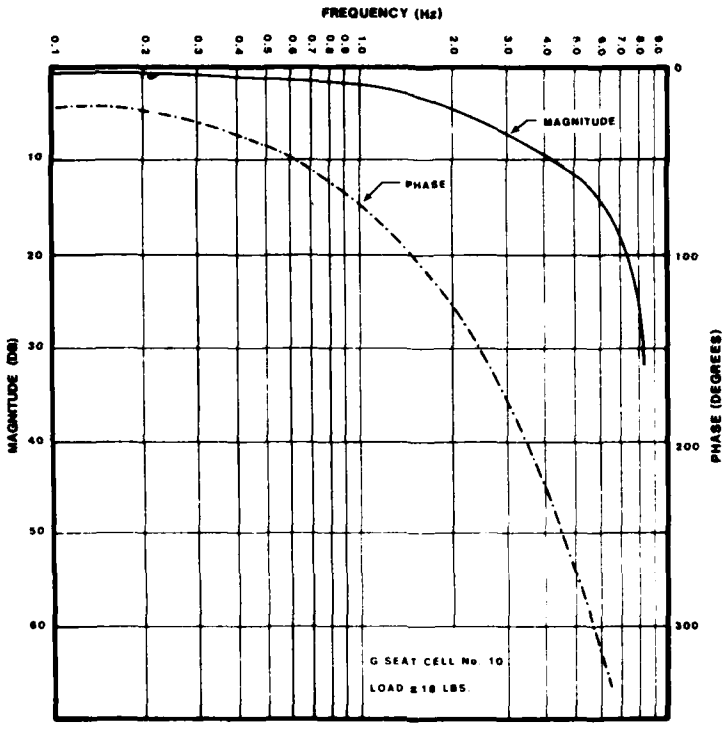


Figure IV-2. Frequency Response of G-Seat Cell With Load

All seat and backrest cells were tested with step inputs to check proper operation. The seat cells were step tested with the 18 lb. load. The backrest cells were tested without a weight other than a light spring attached to the tracking potentiometer. These tests showed consistent and proper operation of all cells. All responses were critically damped with no overshoot.

The throughput lag time for both up and down motion of backrest cell (No. 23) was 70 msec. The 63 percent rise time for up motion was 85-90 msec and for down motion was 65-70 msec. An example of a step response for a seatpan cell (No. 10) is shown in Figure IV-3.

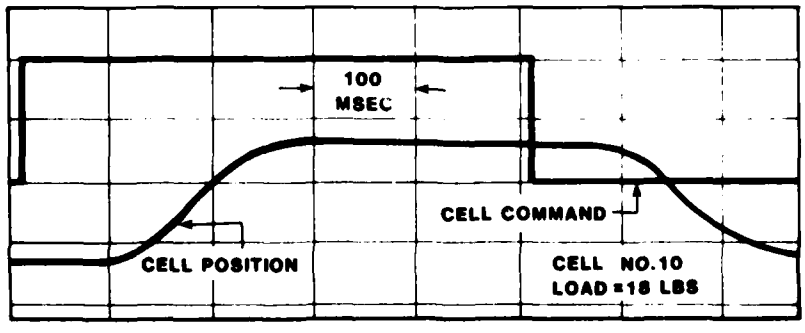


Figure IV-3. Cell Position Response to Step Command

The throughput lag time for the seatpan cell (No. 10) was 85 msec for both up and down motion. Rise time for both up and down motion was 90-100 msec.

# SECTION V

# SYSTEM RESPONSE SUMMARY

A graphic summary of the dynamic response of the VTRS/CTOL computer and hardware systems is presented in Figures V-1 and V-2. Figure V-1 shows performance when operated in a dual mode permitting simultaneous use of the TV model board system and computer image generation (CIG) system. Figure V-2 shows projected performance for a CIG only mode. The system dynamic response is a sum of linkage and computer transport delays and output hardware response time. The output hardware response may contain transport delays and/or signal rise times. Throughput delays are measured from control stick input to output hardware input commands. Aerodynamic and kinematic delays are not included in any of the data presented. Output hardware systems shown in Figure V-1 are all servo controlled devices with the exception of video generation of the CIG picture. Servo response times are defined as the time required for the output to reach 63 percent of the step command. Video generation of the CIG picture includes transport delay within the CIG and a response time defined as the time to complete one TV field.

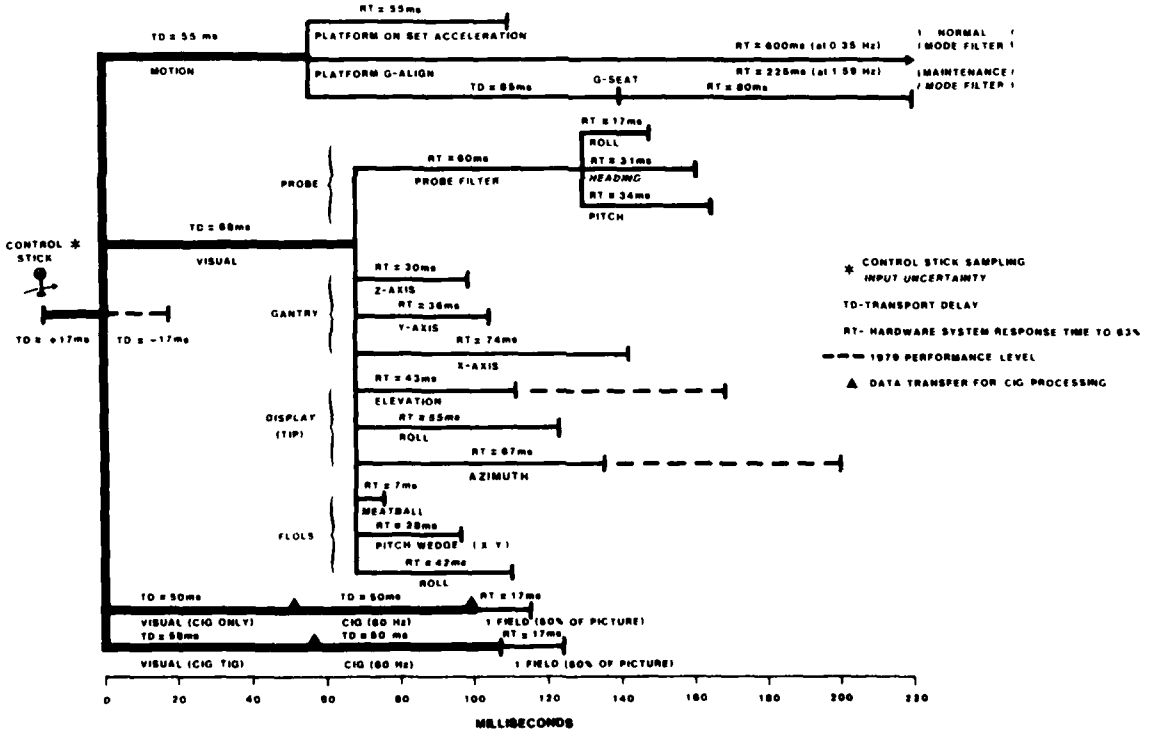


Figure V-1. VTRS Dynamic Response (Model Board TV/CIG)

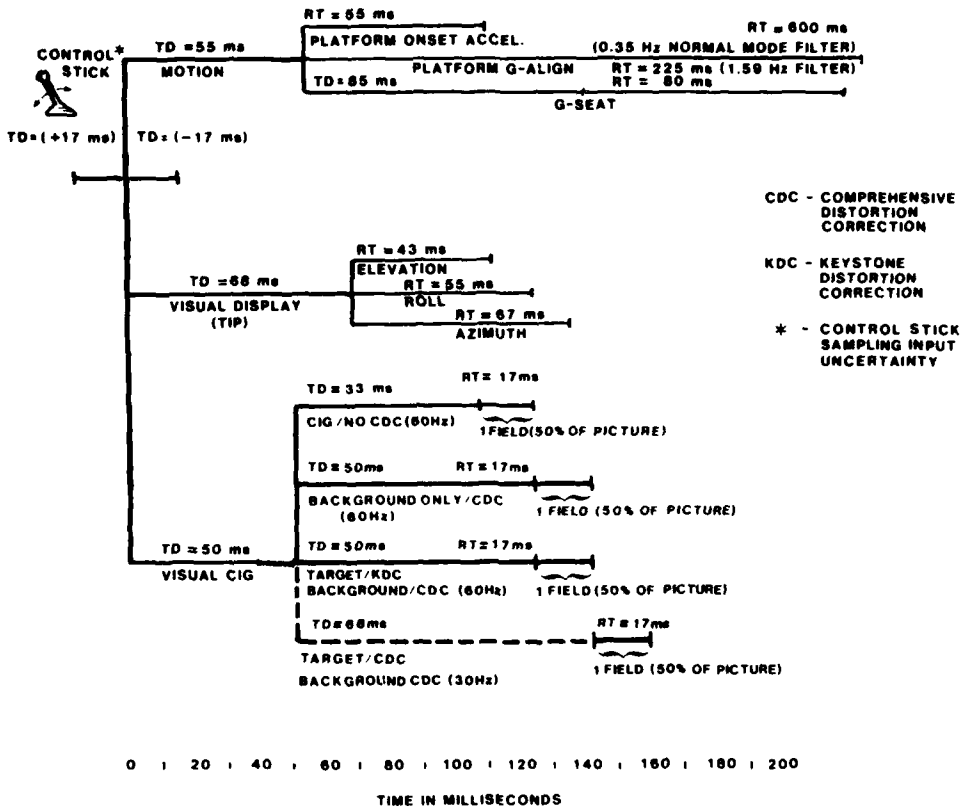


Figure V-2. VTRS Dynamic Response for CIG Systems

Since the control stick input can occur anywhere within a basic computational frame of 33.3 milliseconds duration, timing is referenced to an average between worst case (33.3 milliseconds additional time) and best case (0 milliseconds). Thus, 17 msec is added to the best case and a tolerance of ± 17 msec is placed on system response.

With the exception of the G-seat and G-align systems, the average times for computer throughput plus hardware response for the dual simulation mode of TV model board and CIG is less than 165 milliseconds. However, the G-seat and G-align designs are used for sustained or very low frequency acceleration, and thus do not demand the fast onset cuing. Other G-seat designs which attempt to provide onset cuing would require improved response.

Early tests showed a dynamic mismatch in visual system performance due to poor servo response in the elevation and azimuth target image projector servos. This poor response is shown by dashed lines in Figure V-1. System dynamic mismatch was significantly reduced by design improvements in the elevation and azimuth target projector servos.

From Figure V-1, the system lag (computer transport delay plus hardware rise time) was found to be approximately 120 milliseconds with a tolerance of about ± 20 milliseconds. The probe attitude servos, which are an exception to this, could be readily brought within this tolerance by changing the probe filters. These filters smooth the computer update commands, and are apparently designed for a slower update rate than the 30 Hz used in VTRS.

Figure V-2 summarizes the dynamic response of the VTRS computers, the target image projection system, and motion systems, operating in a CIG only mode. There are four basic simulation configurations while operating in the CIG only mode. These configurations are (1) CIG operating with no comprehensive distortion correction at 60 Hz, (2) background only with comprehensive distortion correction (CDC) updated at a rate of 60 Hz, (3) target with keystone distortion correction (KDC) projected onto a background with CDC, both updated at 60 Hz, and (4) target and background, both with CDC, and both updated at 30 Hz. From Figure V-2 we conclude that the maximum system dynamic response time, including one field of video, is less than 150 milliseconds.

Thus system response times for the dual simulation mode (model board or CIG) or CIG only mode are within guidelines for acceptable simulator performance according to Ricard and Puig (1977).

# SECTION VI

## DESIGN FEATURES SUMMARY

The following design features, incorporated into the VTRS/CTOL simulator, minimized system delays/lags and provided dynamic matching of visual and motion systems:

a. The linkage, which distributes all signals between the computer and simulator systems, has an optimum sequence with respect to its DMA transfer of data between the linkage memory and the computer's memory which occurs near the end of each computation frame. Immediately after this DMA data transfer, all linkage output cards are serviced to minimize output time lag. Then, input cards are serviced and inputs held until the next DMA data transfer to the computer which would be somewhat less than a computation frame time of 33 msec. This type of linkage creates a choice of holding either input data for a frame time as done here or holding output data. In this simulator there are many more time critical outputs than inputs. The delay of critical inputs was overcome by a special servicing of the stick and throttle linkage system card which converts their voltage to a digital word just prior to the DMA transfer of data into the computer. All other inputs have the added frame lag.

b. Since certain flight dynamic outputs such as aircraft position and attitude are required as inputs for visual computations, the visual computational frame (33 msec) must follow the flight computational frame. To minimize any time delays from this, all critical flight subroutines are placed in an optimum calling order and are placed "up front" in the flight computation frame. As a result, the visual computer is phased behind the flight computer by only 16.7 msec, or 1/2 frame rather than waiting 33.3 msec until the next frame.

c. In the "CIG only" mode of operation, subroutines in the visual computer are optimized in calling order for minimization of transport delay As a result, critical visual subroutines are computed at the beginning of the visual computation frame and are bussed to the CIG computers at the end of only one subframe of 8.33 msec.

d. Subroutines computed at rates below the basic 30 Hz of flight and visual, and subroutines that are not a link in the dynamic response chain, are placed towards the end of the computational cycle.

e. The Experimenter Station subroutines are placed in the executive computer and computed in parallel with flight and visual. Thus, they do not add to response time.

f. For smoother visual presentation, the CIG computer is provided with predicted values of eyepoint position/attitude and point-of-interest direction cosines in between actual computed values of these parameters. The net result is a 60 Hz image presentation, with field one generated from computed parameters and field two generated from the predicted parameters.

g. Hardware response of systems such as the target projection servos was increased and then "tuned" such that the times from control stick input to hardware response closely matched the time from stick input to CIG video output.

h. The motion platform acceleration cues lead visual position as in the real world. This desired feature is a result of driving platform position with aircraft acceleration and servicing it with the flight linkage transfer which leads the visual linkage transfer by 16.7 msec.

# REFERENCES

Ricard, G. L. and Puig, J. A., "Delay of Visual Feedback in Aircraft Simulators", NTEC, Orlando, Florida, Tech Note NAVTRAEQUIPCEN TN-56, March 1977.

# APPENDIX A

## TECHNICAL DATA AND ALGORITHMS FOR ACCELERATION CUE GENERATION OF THE MOTION SYSTEM

Acceleration cues are generated by shaping the position response so as to produce the desired acceleration shape, magnitude, duration, etc., as based on the motion platform capabilities.

The scheme does not use position washout and relies on the pilot's desire to return to stable flight. Position washout would require an additional time cycle with an acceleration toward neutral for a time and then a deceleration.

The desired curve of the motion position response is shaped like a second order function with an inflection point occurring at t(cue). Thus, an input step function should be shaped as needed (considering the platform's hardware response) to produce an output position response curve approximating that shown in Figure A-1.

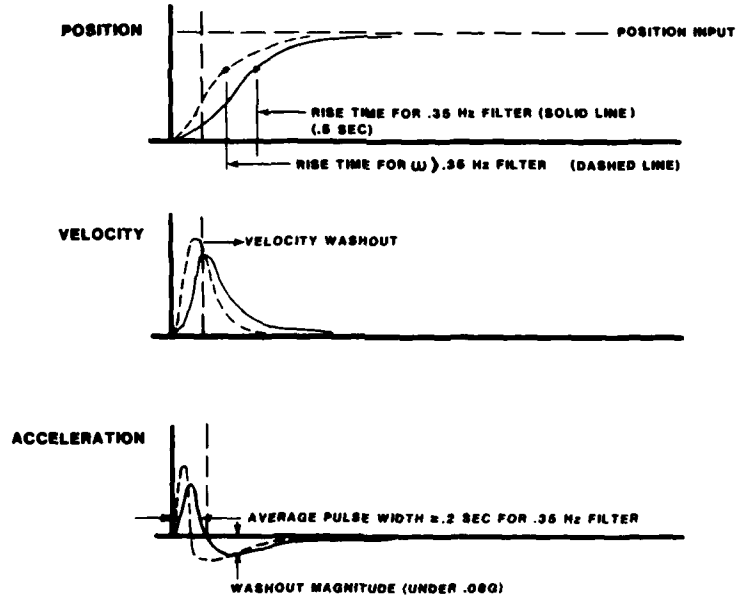


Figure A-1. Effect of Increasing Motion Leg Filter Bandwidth

Command shaping is preferably done in the software prior to the platform leg geometry equations as opposed to shaping the command to each leg. Response consistency is consequenty maintained in each degree of freedom. This minimizes degree of freedom acceleration variations (which are functions of the specific magnitudes of the individual leg commands) even if the range of the commands is within the linear response region. Filtering the motion command inputs in each degree of freedom eliminates the above variations. However, variations resulting from motions exceeding the platform's linear region are not eliminated. Note that if a pitch is commanded within the motion excursion limits, full motion pitch will be obtained. However, if a roll is superimposed, resulting in a total command that exceeds the limits, not only will the roll response be lower than expected, but the pitch will be lower also. Therefore, whenever the motion limits are exceeded, the final response will be a function of the magnitude of all the inputs in all degrees of freedom. The interrelationships and variations can be plotted in families of curves, but cannot be readily summarized. The point of importance is that whenever limits are exceeded, the motion response to an aircraft acceleration is not only a function of the aircraft acceleration inputs and platform gain in a particular degree of freedom, but also acceleration inputs in other degrees of freedom, even those not included as drives.

The shaping of the position drive curve must be tailored as ideally shown in Figure A-1. The VTRS system has characteristics of this form, created by a series of software and hardware filters. Each leg has a second order hardware filter and each rotational degree has a first order software filter. In addition, other special purpose filters such as gravity alignment control are distributed throughout the software. Motion platform block diagrams illustrating this shaping are presented in Figures A-2 through A-7. Software filters are shown in the S, rather than Z domain, for hardware comparison.

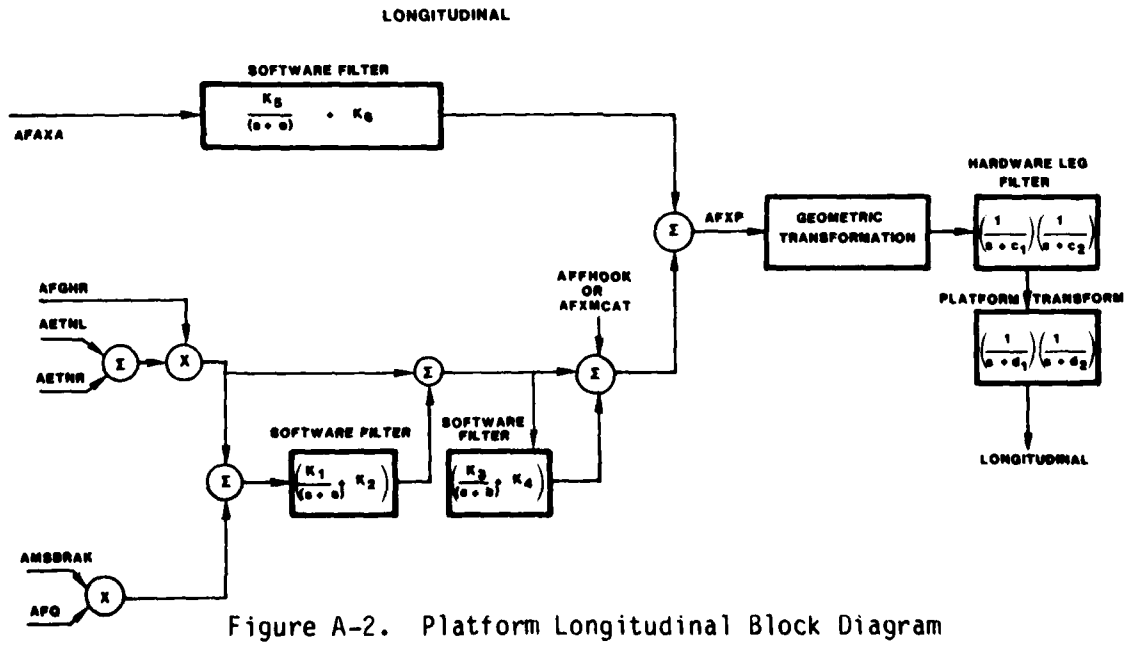


Figure A-2. Platform Longitudinal Block Diagram

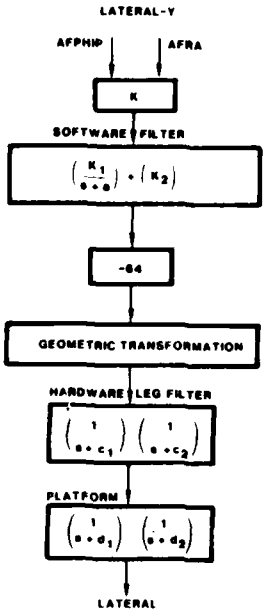


Figure A-3. Platform Lateral Block Diagram

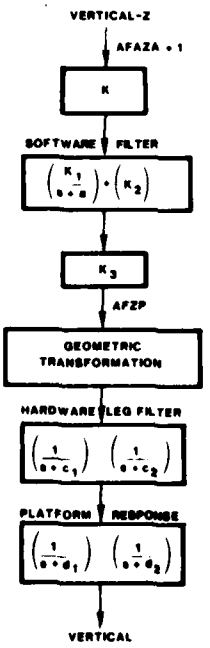


Figure A-4. Platform Vertical Block Diagram

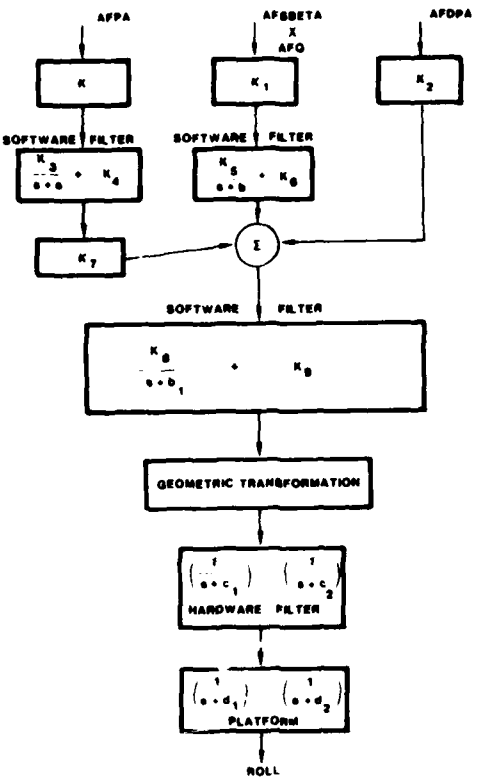


Figure A-5. Platform Roll Block Diagram

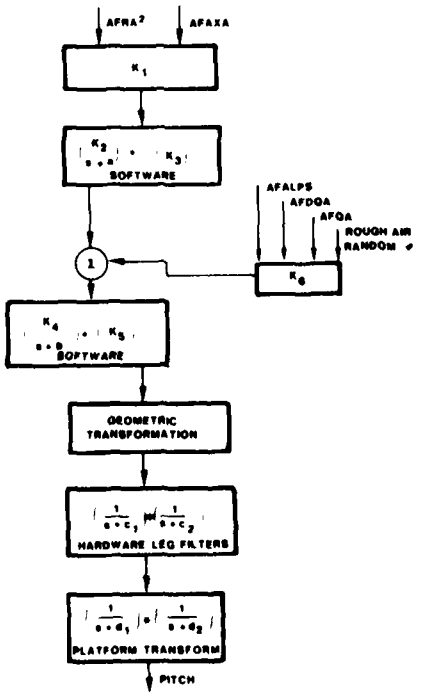


Figure A-6. Platform Pitch Block Diagram

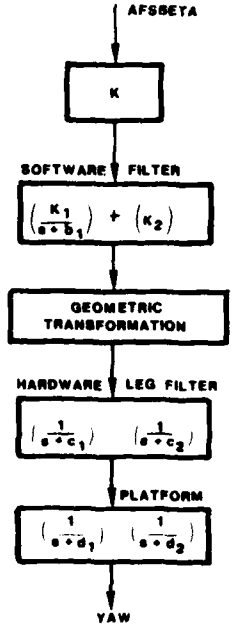


Figure A-7. Platform Yaw Block Diagram

Each of the $(\frac{1}{s+a})$ terms shown in the diagrams is either a first order lag generated by the hardware or a first order lag generated by the software with an initial "jump" at $n = 1$ (first compute cycle).

The first order software lag constant can be compared to a continuous case time constant in the following manner:

$$\text{If } y = x\left[\frac{a}{(s+a)} + K\right]$$

For a step input $x = 1$, $x(s) = 1/s$

$$Y(s) = \frac{a}{s(s+a)} + \frac{K}{s}$$

The solution of which is

$$y = (1 - e^{-at}) + K$$

or after the initial jump,

$$y = (1 - e^{-at})$$

In differential equation form, this solution becomes $\dot{y} + ay = ax$, where a first order backward difference is used to approximate $\dot{y}$:

$$\dot{y} = \frac{y_n - y_{n-1}}{\Delta t}$$

$$y_n - y_{n-1} + a\Delta t y_n = a\Delta t x_n$$

$$y_n(1+a\Delta t) = y_{n-1} + a\Delta t x_n \qquad \Delta t = \text{sample period}$$

Comparing this to the form of

of the software first order filters where

again, after the initial jump:

$$y_n = y_{n-1} + a'(x_n - y_{n-1})$$

or

$$y_n = y_{n-1}(1-a') + a'x_n$$

equating $y_{n-1}$ and $x_n$

$$1-a' = \frac{1}{1+a\Delta t}$$

$$a' = \frac{a\Delta t}{1+a\Delta t}$$

or

$$a' = 1 - \frac{1}{1+a\Delta t} = \frac{1+a\Delta t-1}{1+a\Delta t} = \frac{a\Delta t}{1+a\Delta t}$$

Thus

$$a' = a\Delta t/1+a\Delta t$$

e.g. for $\Delta t = 1/30$ and $a = 1$ (1/time constant)

$$a' = .03225$$

Thus the required a' can be calculated knowing $\Delta t$ and the desired time constant ($\tau$) from

$$a' = \frac{\Delta t/\gamma}{1+\frac{\Delta t}{\tau}} = \frac{\Delta t}{\Delta t+\gamma} \quad \text{where} \quad \gamma = \frac{1}{a}$$

With a simple first order filter, the shaping flexibility is limited. It may be impossible to design a first order filter with a specific 63 percent point and some other desired point such as a 90 percent value. If more flexible shaping is desired, a modified or higher order filter is required.

For example, using the vertical drive equations, a typical lag filter algorithm is as follows:

$$AFZP_n = AFZP_{n-1} + .0322808[1.978K(AFAZA_n - AFAZA_{n-1}) + AFAZA_{n-1} - AFZP_{n-1}]$$

If AFAZA is a constant, then $AFAZA_n = AFAZA_{n-1}$ for $n \geq 1$ and

$$AFZP_n = AFZP_{n-1} + .0322808\ [AFAZA - AFZP_{n-1}].$$

Observe that the typical lag filter with an input that is constant displays an output with an initial jump followed by an exponential decay or rise. To create a second order inflection point, two of these first order filters must be cascaded or a generalized second order must be mechanized.

Observe that in this case, the 1.978 constant determines the initial jump (.063856K (AFAZA)) during the first iteration and thereafter increases to (AFAZA) at a rate determined by the .0322808 constant.

The initial jump via the 1.978K constant determines the initial velocity jump and the .0322808 determines how long it takes to wash the velocity down to zero. This, in turn, determines the velocity washout acceleration as well as the onset acceleration. Note that the onset acceleration occurs during the first iteration and is therefore of too short a duration to be sensed effectively or be of use as an onset, but the washout acceleration can be effectively controlled. Therefore, even with a controllable first order filter such as this, it cannot be used as the acceleration cue shaper. The form of the 1st order motion filters is:

$$Y_n = Y_{n-1} + a\ (X_n - Y_{n-1}) \text{ for } n > 0$$

The response shape to a step input is illustrated in Figure A-8.

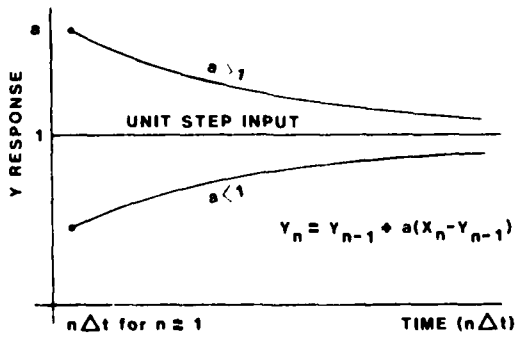


Figure A-8. First Order Filter Response

The general form of the software filters used herein to provide for the controllability of the jump magnitudes and delay rates.

$$y_n = y_{n-1} + b[a(x_n - x_{n-1}) + x_{n-1} - y_{n-1}]$$

The position response for a step input for (a) < 1, (ab) > 1 and (ab) < 1 is illustrated in Figure A-9.

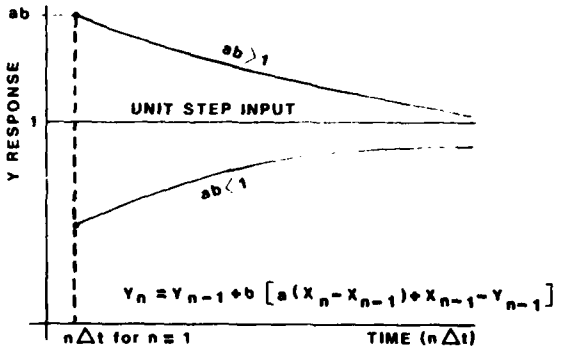


Figure A-9. Position Response for Step Input

The velocity and acceleration outputs for a typical filter used in this system are presented in Figure A-10. The duration of velocity and acceleration can be expanded by the properties of the filter.

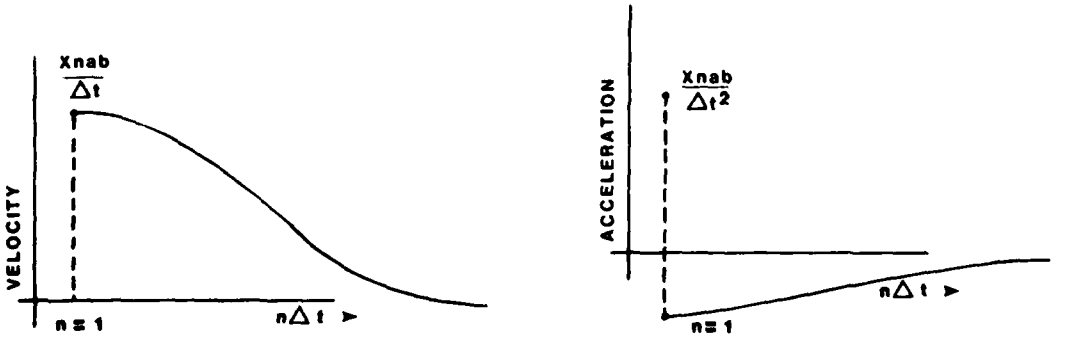


Figure A-10. Typical Filter Velocity and Acceleration Outputs

When the above digital filter output is used to command a platform with a typical frequency response and no hardware filter, it will result in a platform response as illustrated in Figure A-11.

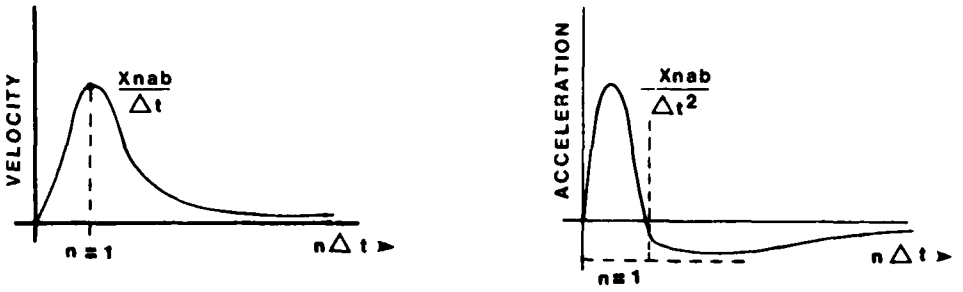


Figure A-11. Onset Cue Velocity and Acceleration Response

Observe from Figure A-11 that the onset acceleration response to a step input is too rapid to be usefully felt.

Excessively high frequencies are passed, causing acceleration spikes at the iteration rate frequencies (30 Hz).

To ensure the required minimum acceleration cue time and provide for filtering of the 30 Hz sample noise, hardware filters are provided in the input to the platform leg servos.

To determine the motion platform hardware response characteristics, the platform was driven in heave with an analog step command to the leg filters. Heave was selected because a maximum platform load is driven in that axis and a single axis motion can be achieved without driving through software.

A block diagram of this test set-up is shown in Figure A-12. Each leg servo is essentially identical and each leg command is driven through a second order passive linear filter. The form of this filter and its transfer function are shown in Figure A-12. This command filter is overdamped, has a rise time of 0.5 seconds and a bandwidth (-3 db) of 0.35 Hz.

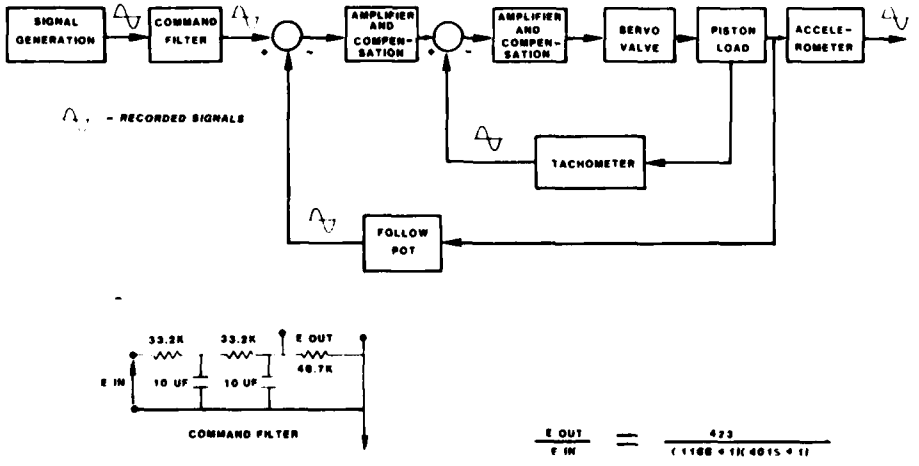


Figure A-12. Motion System Test Diagram

Closed loop frequency response plots of the motion system with and without the influence of the command filter are presented in Figure A-13. Note that the command filter response and the motion system response (including filter) are approximately the same. The command filter clearly dominates the dynamic character of the motion system.

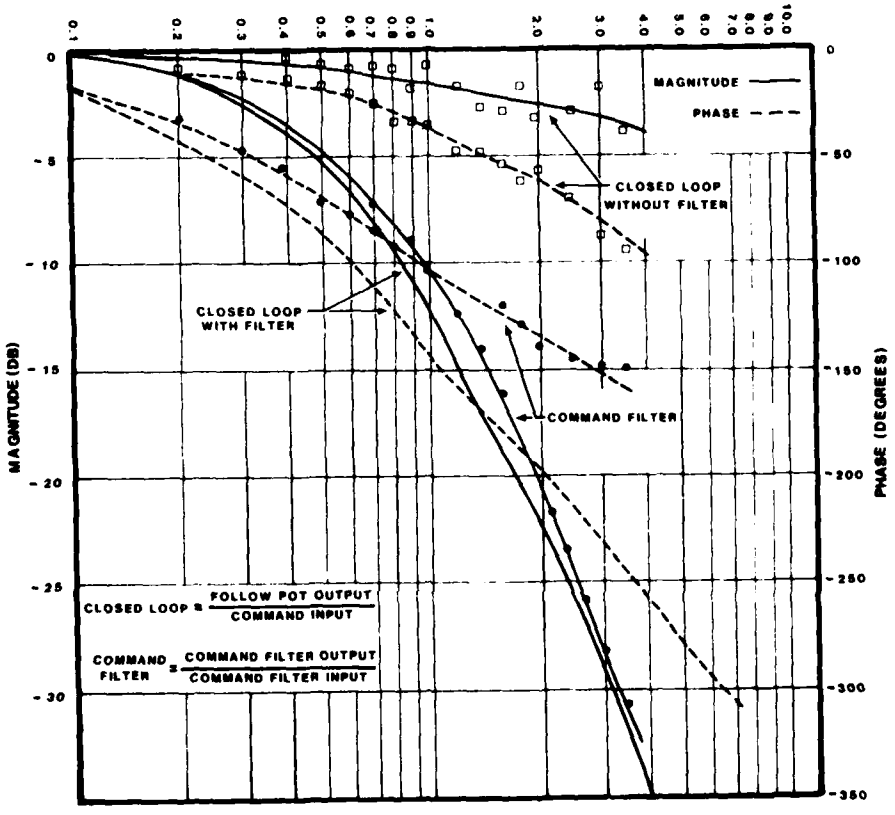


Figure A-13. Motion System Frequency Response

Motion algorithms, designed to provide the onset acceleration and washout the sustained (low frequency) components, are of the basic form:

$$X_c = KX_{a/c} + f \text{ (other terms)}$$

where

$K$ = constant (displacement/accel)

$X_c$ = displacement command to motion system

$X_{a/c}$ = aircraft acceleration

If the motion system is assumed to have a second order transfer characteristic,

$$\frac{X_b}{X_c} = \frac{1}{1+2\zeta/\omega_o S + S^2/\omega_o{}^2} \qquad S = \frac{d}{at}$$

$\zeta$ = damping ratio

$\omega_o$ = natural frequency

$X_b$ = motion base displacement

$X_c$ = displacement command to motion base

Then, using the motion algorithm, we get

$$\frac{\ddot{X}_b}{\ddot{X}_{a/c}} = \frac{KS^2}{1+2\zeta/\omega_o S + S^2/\omega_o{}^2}$$

This is the transfer function between motion base acceleration and aircraft acceleration. Figure A-14, a simplified frequency plot of this TF, illustrates that it will pass the onset acceleration ($\omega>\omega_o$) and will reject the sustained acceleration ($\omega<\omega_o$). It is, in effect, the acceleration washout filter.

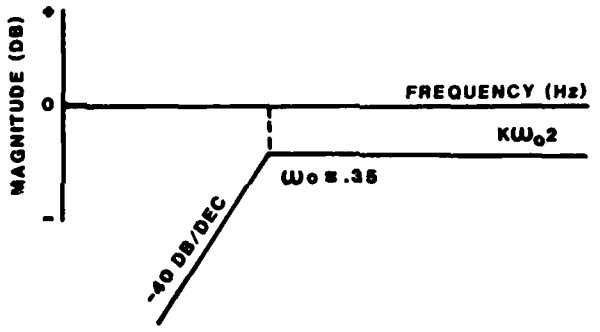


Figure A-14. Frequency Response of Motion Base Acceleration Onset Cue

Note that the break frequency defining washout depends on the bandwidth ($\omega_o$).

Tests to determine the character of the onset and subsequent washout of acceleration were performed by issuing step commands in position (heave, in this case). Typical responses to these step commands are shown in Figure A-15. The command, position follow pot, command filter output, and

acceleration histories are also shown in the figure. The peak heave command of 3.2 inches resulted in a peak acceleration of 0.2G's. The reversing acceleration, an undesirable cue, is about 20 percent of the desired acceleration. Washout of the sustained acceleration is observed to take approximately 1 second.

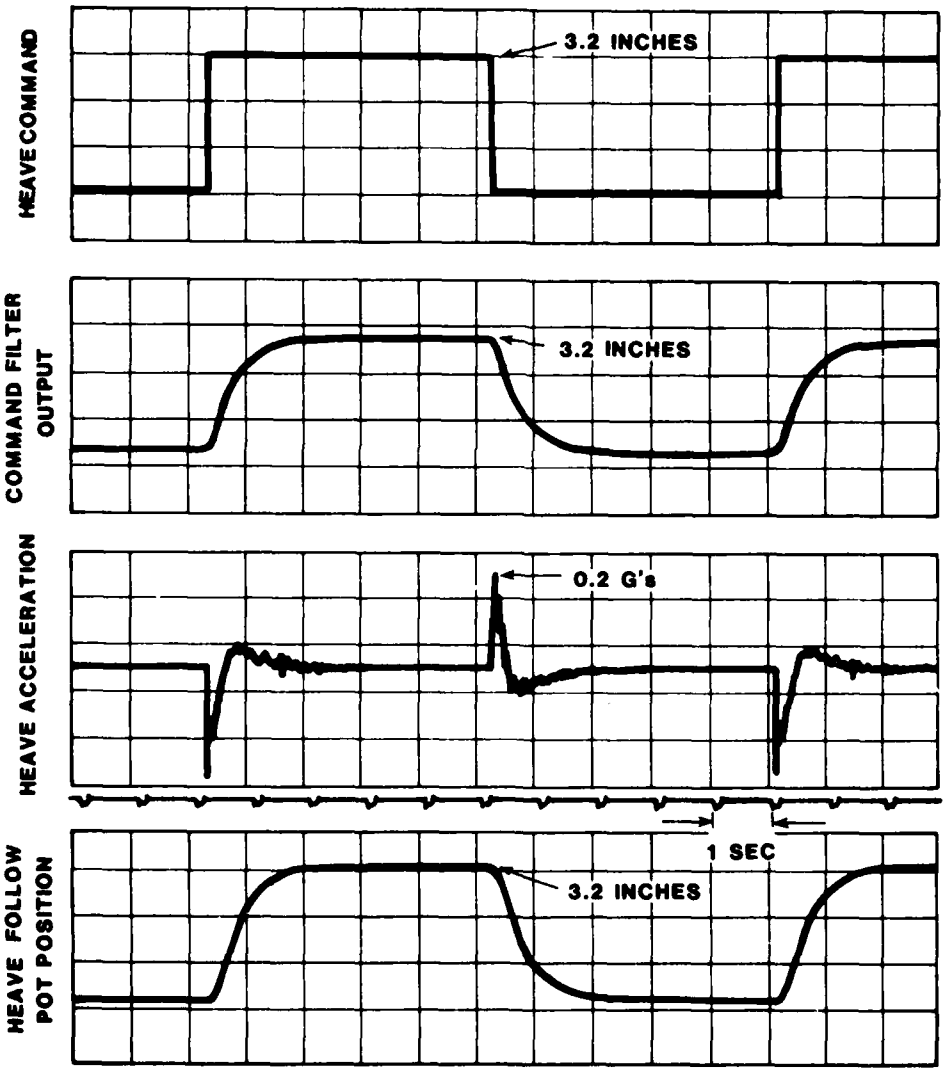


Figure A-15. Motion System Heave Step Response

The platform bandwidth without filtering is approximately 2.5 Hz. With .35 Hz filtering, the magnitude response as a function of frequency can be generalized into a gravity align and acceleration cue response that functions approximately as follows.

For gravity align, an aircraft acceleration generates a proportional command of platform position as shown in Figure A-16.

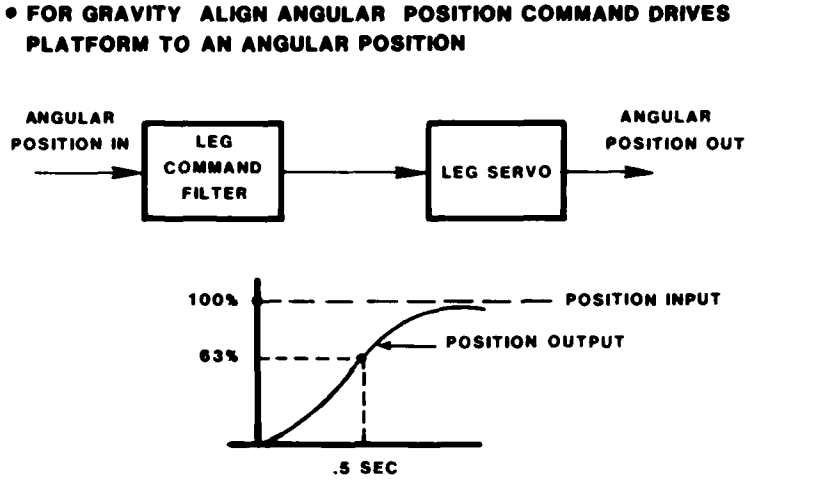


Figure A-16. Gravity Align

The generalized slope of the frequency response function is shown in Figure A-17.

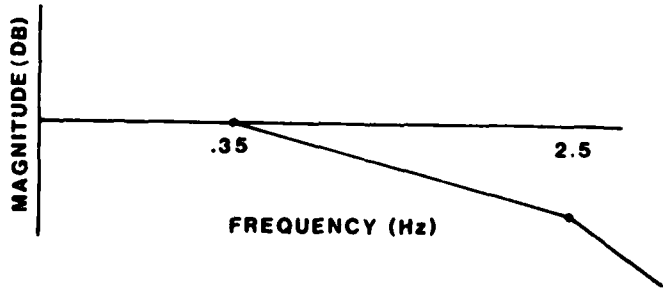


Figure A-17. Generalized Gravity Align Frequency Response

For acceleration cuing, aircraft acceleration generates a proportional command of platform position to achieve platform acceleration as shown in Figure A-18.

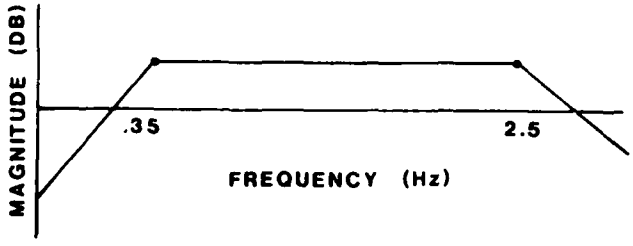


Figure A-18. Generalized Frequency Response for Acceleration Onset

Observe that for acceleration onset, low frequencies are filtered to provide rapid onset and washout. High frequencies are filtered to prevent stepping and spurious influences, thereby providing a smooth, controlled magnitude and duration of onset and washout.

For gravity align, low frequencies are passed and high frequencies are filtered. The high frequency longitudinal accelerations which are simulated by pitch are not passed. Since those high frequencies are passed in the longitudinal acceleration cue simulation, they are not required to be duplicated in the gravity align portion.

The software and hardware filters are designed to operate together, each performing their specified functions. The software filters provide for flexible setting of gains and washout rates while the hardware filters provide cue shaping and smoothing. The platform, with a bandpass of approximately 2.5 Hz, is fast enough to respond to a 30 Hz iteration rate. Adding the hardware filter attenuates the high frequency range to create a selective broadening of the acceleration pulse to provide a minimum cue duration for steady state inputs. In addition, this same filter passes the low frequencies for position, allowing the proper simulation of gravity align.

The transport delay and filter effects of the motion system are summarized in Figure A-19. The overall system was tested for throughput lag which includes transport lag (dead time to response) and 63 percent system response time. The motion system data is presented in Section III. It should be noted that the motion overall lag will vary depending on the drive philosophy. For example, the system lag for gravity align is much greater than for acceleration cuing since it does not include the lead acquired by the acceleration cue method of reading actual platform acceleration. This lag is deliberate and must be optimized to be neither too fast nor too slow.

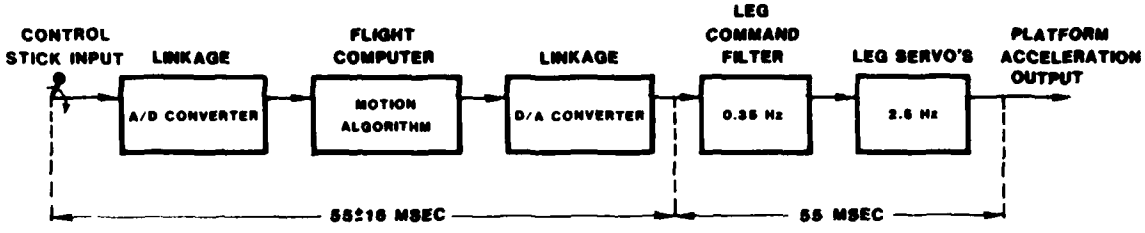


MAGNITUDE OF ACCELERATION OUTPUT CAN BE INCREASED BY:

a) INCREASING SOFTWARE GAIN

b) *INCREASING LEG FILTER CUTOFF FREQUENCY; HOWEVER,* THIS OPTION WILL DECREASE ACCELERATION PULSE DURATION. PRESENT PULSE WIDTH IS APPROXIMATELY= 200 MSEC (CUE SENSING THRESHOLD).

Figure A-19. Onset Acceleration Performance

DISTRIBUTION LIST

| | | | |
|---|---|---|---|
| Naval Training Equipment Center<br>Orlando, Florida 32813 | 60 | AFOSR/NL (Dr. A. R. Fregley)<br>Bolling AFB<br>Washington, D.C. 20332 | 1 |
| Commander<br>HQ, TRADOC<br>Attn: ATTNG-PA<br>Ft. Monroe, Virginia 23651 | 1 | Library<br>Division of Public Documents<br>Government Printing Office<br>Washington, D.C. 20402 | 1 |
| Center Library<br>Naval Personnel Research and Development Center<br>San Diego, California 92152 | 2 | Director<br>Training Analysis & Evaluation Group<br>Department of the Navy<br>Orlando, Florida 32813 | 2 |
| Dr. Ralph R. Canter<br>U.S. Army Research Institute<br>Field Unit<br>P. O. Box 16117<br>Fort Harrison, Indiana 46216 | 1 | HumRRO/Western Division/Carmel Office<br>27857 Berwick Drive<br>Carmel, California 93923 | 1 |
| Defense Technical<br>Information Center<br>Cameron Station<br>Alexandria, Virginia 22314 | 12 | U.S. Coast Guard (G-P-1/62)<br>400 Seventh Street, SW<br>Washington, D.C. 20590 | 1 |
| AFHRL Technology Office<br>Attn: MAJ Duncan L. Dieterly<br>NASA-Ames Research Center<br>MS 239-2<br>Moffett Field, California 94035 | 1 | National Aviation Facilities<br>Experimental Center<br>Library<br>Atlantic City, New Jersey 08405 | 1 |
| Commanding Officer<br>Air Force Office of Scientific Research<br>Technical Library<br>Washington, D.C. 20301 | 1 | AFHRL/TSZ<br>Brooks AFB, Texas 78235 | 1 |
| OUSDR&E (R&AT) (E&LS)<br>CDR Paul R. Chatelier<br>Room 3D129, The Pentagon<br>Washington, D.C. 20301 | 1 | Chief<br>ARI Field Unit<br>P. O. Box 476<br>Ft. Rucker, Alabama 36362 | 1 |

DISTRIBUTION LIST (cont'd)

Dr. Jesse Orlansky 1
Science and Technology Division
Institute for Defense Analyses
400 Army-Navy Drive
Arlington, Virginia 22202

Chief of Naval Operations 1
OP-987H
Attn: Dr. R. G. Smith
Washington, D.C. 20350

Scientific Technical Information Office 1
NASA
Washington, D.C. 20546

Dr. J. M. Rolfe 1
Research Branch
Hq. RAF Support Command
RAF Upwood
Huntington, Cambs UK

Chief of Naval Operations 1
OP-115
Attn: M. K. Malehorn
Washington, D.C. 20350

Technical Library 1
Naval Training Equipment Center
Orlando, Florida 32813

Chief of Naval Operations 1
OP-596
Washington, D.C. 20350

Commander 1
Naval Air Test Center
CT 176
Patuxent River, Maryland 20670

Technical Library 1
OUSDR&E
Room 30122
Washington, D.C. 20301

Commander 2
Naval Air Systems Command
AIR 340F
Attn: CDR C. Hutchins
Washington, D.C. 20361

Capt. A. Ginsburg 1
Aviation Vision Laboratory
AFAMRL/HEA
WPAFB, Ohio 45433

Mr. Ken Staples 1
Flight Research Division
Royal Aircraft Establishment
Bedford MK41 6AE UK

Dr. Martin Tolcott 1
Office of Naval Research
800 N. Quincy Street
Department of the Navy
Arlington, Virginia 22217

Commander 1
Naval Air Development Center
Attn: Technical Library
Warminster, Pennsylvania 18974

Naval Research Laboratory 1
Attn: Library
Washington, D.C. 20375

Chief of Naval Education and Training 6
Liaison Office
AFHRL/OTLN
Williams AFB, Arizona 85224

DISTRIBUTION LIST (cont'd)

Office of Deputy Chief of Naval Operations
Manpower, Personnel and Training (OP-01)
Washington, D.C. 20350 — 1

Assistant Secretary of the Navy
Research, Engineering & Systems
Washington, D.C. 20350 — 1

HQ Marine Corps
Code APC
Attn: LTC J. W. Biermas
Washington, D.C. 20380 — 1

Chief of Naval Operations
OP-593B
Washington, D.C. 20350 — 1

Scientific Advisor
Headquarters U.S. Marine Corps
Washington, D.C. 20380 — 1

Commander
Pacific Missile Test Center
Point Mugu, California 93042 — 1

Commander
Naval Air Systems Command
AIR 413
Washington, D.C. 20361 — 1

Commanding Officer
Naval Aerospace Medical Research Laboratory
Code L5
Department of Psychology
Pensacola, Florida 32512 — 1

Dr. Donald W. Connolly
Research Psychologist
Federal Aviation Administration
FAA NAFEC ANA-230 Bldg. 3
Atlantic City, New Jersey 08405 — 1

Chief of Naval Material
MAT 08D2
CP5, Room 678
Attn: Arnold I. Rubinstein
Washington, D.C. 20360 — 1

Commanding Officer
Naval Education Training Program and Development Center
Attn: Technical Library
Pensacola, Florida 32509 — 1

Commander
Naval Air Systems Command
Technical Library
AIR-950D
Washington, D.C. 2036. — 1

Chief of Naval Education and Training
Code 01A
Pensacola, Florida 32509 — 1

Dr. David C. Nagel
LM-239-3
NASA Ames Research Center
Moffett Field, California 94035 — 1

Federal Aviation Administration
Technical Library
Bureau Research & Development
Washington, D.C. 20590 — 1

Commander
Naval Weapons Center
Human Factors Branch (Code 3194)
Attn: Mr. Ronald A. Erickson
China Lake, California 93555 — 1

DISTRIBUTION LIST (cont'd)

Dr. Thomas Longridge 1
AFHRL/OTR
Williams AFB, Arizona 85224

Dr. Kenneth Boff 1
ARAMRL/HEA
Wright Patterson AFB, Ohio 45433

CAPT James Goodson 1
Code L-32
Naval Aerospace Medical Research
Laboratory
Pensacola, Florida 32512

Dr. Genevieve Haddad 1
AFOSR/NL
Bolling AFB, D.C. 20332

Mr. Don Gum 1
AFWAL/FIGD
Wright Patterson AFB, Ohio 45433

Mr. James Basinger 2
ASD/YWE
Wright Patterson, AFB, Ohio 45433

Mr. Rowland Bowles 1
NASA Langley Research Center
MS 125-B
Hampton, Virginia 23365

Mr. Robert Wright 1
Aeromechanics Lab
(USAAVRADCOM)
Ames Research Ctr, MS 239-2
Moffett Field, California 94035

Lt Col Jefferson Koonce 1
USAFA/DFBL
USAF Academy, Colorado 80840

CDR Joseph Funaro 1
Code 602
Human Factors Engineering Division
Naval Air Development Center
Warminster, Pennsylvania 18974

Dr. Will Bickley 1
USARI Field Unit
P.O. Box 476
Fort Rucker, Alabama 36362

Mr. Brian Goldiez 1
PM TRADE
DRCPM-PND-RE
Naval Training Center
Orlando, Florida 32813

Mr. David L. Key 1
U.S. Army AVRADCOM, M.S. 215-1
Ames Research Center
Moffett Field, CA 94035

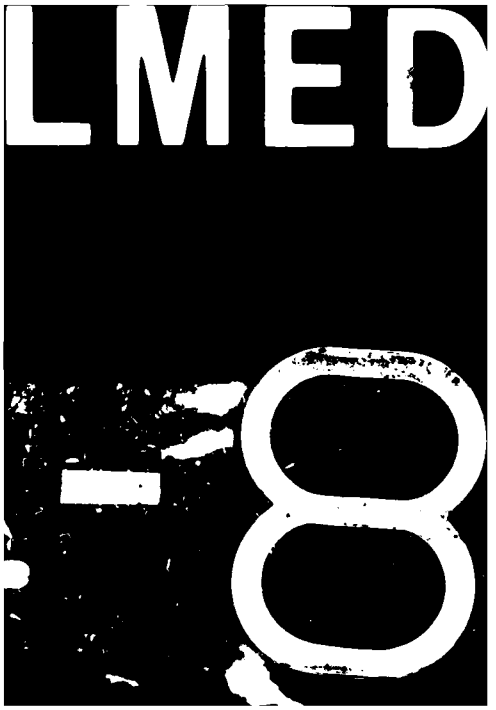
LMED
8